2020

Nanoconjugation; a case study towards improving nanoparticle-based therapeutics

BOSTON UNIVERSITY

GRADUATE SCHOOL OF ARTS AND SCIENCES

Dissertation

NANOCONJUGATION;
A CASE STUDY TOWARDS IMPROVING
NANOPARTICLE-BASED THERAPEUTICS

by

ALI KHANEHZAR

B.S., Shiraz University, 2008
M.S., Amirkabir University of Technology (Tehran Polytechnic), 2011

Submitted in partial fulfillment of the

requirements for the degree of

Doctor of Philosophy

2020

Approved by

First Reader

Björn Reinhard, Dr. rer. nat.
Professor of Chemistry
Professor of Materials Science and Engineering

Second Reader

Sam Thiagalingam, Ph.D.
Associate Professor of Medicine
Associate Professor of Genetics and Genomics
Associate Professor of Pathology & Laboratory Medicine

Third Reader

Lawrence D. Ziegler, Ph.D.
Professor of Chemistry
Professor of Materials Science and Engineering

Fourth Reader

Mark W. Grinstaff, Ph.D.
Distinguished Professor of Translational Research
Professor of Chemistry
Professor of Biomedical Engineering
Professor of Materials Science and Engineering
Professor of Medicine

NANOCONJUGATION; A CASE STUDY TOWARDS IMPROVING NANOPARTICLE-BASED THERAPEUTICS

ALI KHANEHZAR

Boston University Graduate School of Arts and Sciences, 2020

Major Professor: Bjoern Reinhard, Professor of Chemistry

ABSTRACT

Nanoparticles (NPs), nanometer scale materials possessing intriguing novel properties different from that of bulk materials of same nature, are proving to have a prodigious potential not only for improving current therapeutics but also for modulating fundamental processes of living organisms in the nanometer scale. Covalent attachment of a biological functionality to NPs, i.e. nanoconjugation, has, in fact, provided new opportunities for controlling and enhancing the function of molecular functionalities tethered to NPs.

Epidermal Growth Factor (EGF), a growth factor known to signal for cell growth after binding to EGF receptor (EGFR), has been indicated to enhance EGFR-mediated apoptosis in nanoconjugated form in EGFR-overexpressing cancer cells. Many aspects of the induction of apoptosis through nanoconjugated EGF remain, however, insufficiently understood. To address this knowledge gap, the work described in this thesis investigates the role of physicochemical NP properties, such as size, shape, core material composition, and EGF surface loading in enhancing EGF-mediated apoptosis in breast cancer cells. In particular, this thesis aims to elucidate the mechanism(s) through which nanoconjugation

changes the outcome of intracellular EGF-initiated cell signaling from cell growth and proliferation to apoptosis in EGFR-overexpressing breast cancer cells.

Data are presented that demonstrate that spherical NP-EGF with a diameter of 80 nm in core size show the highest efficacy in enhancing EGF-mediated apoptosis. These NPs were found to switch the outcome of EGFR signaling from growth and proliferation to apoptosis by modulating EGFR-mediated generation and activity of intracellular signaling molecules, such as reactive oxygen species (ROS) and Mitogen-activated protein kinases (MAPKs) family enzymes, in particular, c-Jun N-terminal kinases (JNKs). Intriguingly, it was found that nanoconjugated EGF was particularly effective in inducing apoptosis in difficult-to-treat EGFR-overexpressing basal-like breast cancer cells known for poor prognosis. Furthermore, some experimental observations indicate that nitric oxide inhibitors and NP-EGF show potential to synergistically enhance EGF-mediated apoptosis. This finding suggests a potential cell protective role for the EGFR-induced nitric oxide generation and introduces a potential therapeutic approach to improve cancer therapeutics.

Back and forth, up and down, Paving the path, explore, red to violet, wisdom of the ages, to follow or to create, unity of consciousness, what time is it?, synchronizing with the wise, citizens of the universe, wish, beyond the time limits …

Sincerely,

Ali Khanehzar

Table of Contents

LIST OF FIGURES

1 Chapter 1

Introduction, and significance

1.1 Nanoparticle (NP) definition, history

NPs or ultrafine particles are usually referred to particles with a size in the range of 1 to 100 nano-meters (nm). Interest in NPs arises from the novel properties of materials at nanoscale which differentiate them from bulk materials [1]. However, NPs are not necessarily materials in the range of 1 to 100 nm, but novel properties at nanoscale which is not observed in bulk materials is what defines them rather than their size. Surprisingly, NPs are not the result of modern research, and the history of metallic NPs with interesting optical properties goes back to many centuries ago with decorating applications in glassware; an example is use of gold NPs in the famous Lycurgus Cup manufactured by Romans in the 4th century [2] (figure 1). The emergence of nanotechnology goes back to 150 years ago when Michael Faraday presented his research on 'Experimental Relations of metals to Light' to the Royal Society of London.[1] The origin of modern nanotechnology is believed to be from Richard Feynman, "the 1965 noble prize laureate in physics". "There is plenty of room at the bottom" is the title of a lecture he presented at American Physical Society in 1959, when he proposed the idea of manipulating materials at atomic scale. The idea of synthesizing and manipulating nano-scale materials was further developed and found a huge interest in the 21st century expressing the potential of nanomaterials to study and solve fundamental processes of living creatures with applications in the area of "nano-medicine". Some main applications of nanomaterials in nanomedicine will be introduced here.

[1] M. Faraday Philos. Trans. R Soc. Lond., 147 (1857), p. 145

Fig. 1-1 Use of gold NPs in Lycurgus Cup manufactured by Romans in the 4th century [2].[2]

1.2 NPs application in biology and medicine

One outstanding property of NPs is their comparable size with biomolecules and biological entities (virus, cells, and biomolecules) making them a great candidate for biological applications such as Bioanalytical assays, that use NPs as labels to detect and study cells, proteins, nucleic acids, and lipids [3]–[6], or separation and purification of biomolecules by utilizing magnetic NPs.

Perhaps the most significant application of nanotechnology is nanomedicine, "a branch of medicine that applies the knowledge and tools of nanotechnology to the prevention and treatment of diseases. Nanomedicine involves the use of nanoscale materials, such as biocompatible NPs and nanorobots, for diagnosis, delivery, sensing or actuation purposes in a living organism."[3] NP-based drug delivery is a subcategory of nanomedicine which

[2] Reprinted from publication title "The fascinating world of nanoparticle research," vol. 16, no. 7–8, pp. 262–271, 2013. F. J. Heiligtag and M. Niederberger, Mater. Today, copyright (2013) with permission from Elsevier

[3] https://www.nature.com/subjects/nanomedicine

has been studied with an increasing rate recently due to capability of NPs to reduce drug toxicity by targeting specific cells/organs and increasing drug bioavailability.

Utilizing NPs for drug delivery is of great interest for the following main reasons:

NPs can be engineered in a way to mimic biological entities to reduce toxicity and immunogenic responses. NPs are capable of reducing toxicity of drugs through passive or active targeting to the desired body tissues [12], [13]. NPs can protect molecules such as nucleic acids from biodegradation by encapsulation, and enhance their delivery and availability to desired cells and related organelles [14]–[16]. Due to novel properties of nanoscale materials, NPs can enhance drug efficacy by modulating cellular processes such as endocytic pathways [17]–[21] and downstream signaling [22]–[24].

Despite huge potential for addressing longstanding health-related challenges, NPs can themselves cause or enhance toxicity due to nano-scale specific properties. The difference between bulk and nanomaterials necessitates more fundamental studies into their interactions with biological entities. The obtained gain in knowledge could be utilized to tune their properties to specific applications such as terminating cancer cells or delivering therapeutics selectively to diseased cells.

1.3 NPs to explore fundamental properties of living organisms

NPs with comparable size with biomolecules are potential tools to explore and study fundamental properties of living cells/organisms. For instance, the large optical cross-

section of noble metal NPs with localized plasmons and their ability to couple has been utilized to study cell surface membrane receptors organization [7], [8]. Importantly, NPs can be engineered to mimic pathological entities, such as viruses. These NPs are precision model systems to study their pathological behavior under defined conditions. This approach can lead to new therapeutic strategies to fight viral diseases [9]–[11]. We can, however, not only obtain a greatly improved understanding of how mother nature behaves, but also finding new therapeutic strategies for a variety of diseases.

1.4 NPs application in treatment of cancer

1.4.1 What is cancer?

Cancer is a disease which is related to abnormal uncontrollable growth and proliferation of the cells in the body capable of destroying body tissues. Cancer originates from genetic abnormalities inherited from parents or caused by damage to DNA during lifetime.[4] If not prevented, and not diagnosed early, cancer can lead to serious health issues and ultimately death which further shows the significance of attention to this specific disease.

1.4.2 What is Breast cancer and why does it need attention?

Breast cancer is a type of cancer that originates from breast cells. “Breast cancer is the second most common cancer in women and men **worldwide**. In 2012, it represented

[4] https://www.cancer.gov/about-cancer/understanding/what-is-cancer

about 12 percent of all new cancer cases and 25 percent of all cancers in women." "Since 2008, worldwide breast cancer incidence has increased by more than 20 percent. Mortality has increased by 14 percent."[5]

These statistics fully clarifies the significance of further studies for developing therapeutics for (breast) cancer treatment.

1.4.3 Classification of breast cancer cells?

Breast cancer cells can be classified into 4 main categories:

1) Luminal A
2) Luminal B
3) Triple negative/basal like
4) HER2 enriched

Among these cell lines, Luminal types grow more slowly and are known for relatively better prognosis, in contrary to basal like breast cancer cell lines (BLBCs) with higher growing rate and poor prognosis. Although there has been a significant advance in cancer therapeutics in recent years, treatment remains challenging especially for aggressive, metastatic cancer cells with poor prognosis. The main challenge here, is difficult-to-treat BLBCs due to their lack of estrogen receptor, progesterone receptor and HER2 that makes them more difficult to treat and target [25]. Here, new therapeutic

[5] https://www.bcrf.org/breast-cancer-statistics

strategies that can overcome these biologic barriers to **terminate/normalize** cancer cells will be of great significance.

1.4.4 NPs as delivery systems for cancer treatment

NPs are capable of contributing significantly not only by reducing drug side effects and non-specific toxicity to normal cells but also due to their capability of accumulating in tumors through a natural process called EPR (the enhanced permeability and retention) (figure 1-2) i.e. the concept of passive targeting [26]–[28]. In addition, NPs surface properties can easily be engineered with desired ligands facilitating more specific and efficient targeting to tumor sites, i.e. the concept of active targeting [29]–[32].

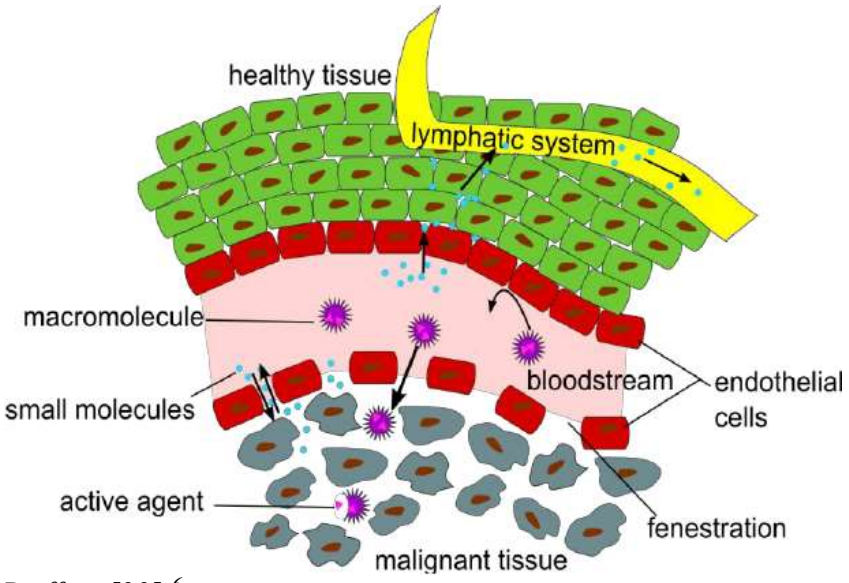

Fig. 1-2 EPR effect [33].[6]

[6] Reprinted from publication title Radiolabeling of Nanoparticles and Polymers for PET Imaging. Stockhofe K, Postema JM, Schieferstein H, Ross TL. Pharmaceuticals (Basel, Switzerland). 2014 ;7(4):392-418. DOI: 10.3390/ph7040392. Copyright (2014).

1.5 Epidermal Growth Factor Receptor (EGFR) as a target to treat cancer cells

1.5.1 What is EGFR? [7]

EGFR, 134 KDa in MW, is a cell surface membrane receptor which signals for cell growth, proliferation, and apoptosis inhibition upon binding to EGF, a growth factor and peptide about 6.2 KDa in molecular weight. Upon binding to EGF, EGFR undergoes a conformational change, dimerizes and crossphosphorylates tyrosine kinases located in the cytoplasmic domain of the receptor initiating a cascade of phosphorylation reactions and downstream signaling that leads to gene transcription in the nucleus (figure 3) [34], [35].

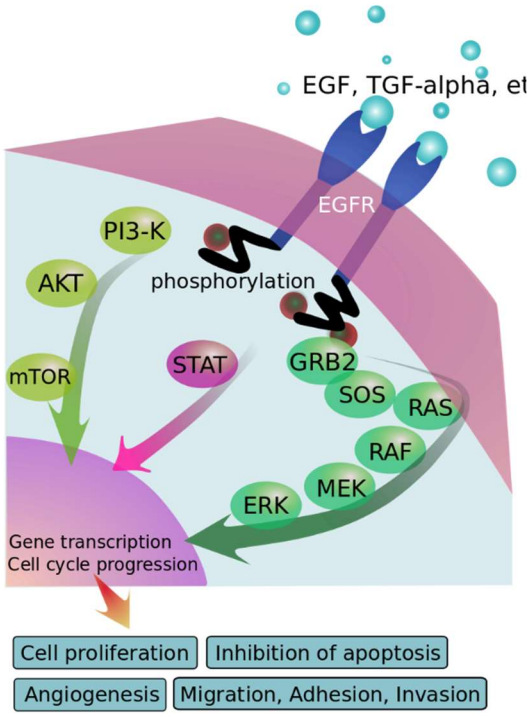

Fig. 1-3 EGFR signaling (Wikipedia.com)

1.5.2 EGFR signaling in cancer

EGFR is overexpressed in many cancer cell lines [36]–[40] which makes it a potential target molecule to deliver therapeutics to cancer cells. It has been shown that EGFR can signal for apoptosis in EGFR overexpressing cell lines if exposed to high doses of EGF [41]–[45], indicating EGFR overexpression as a property of most cancer cells that

[7] Figure 3: https://en.wikipedia.org/wiki/Epidermal_growth_factor_receptor. Copyright.

can be utilized and even further enhanced against them. In fact, activated EGFR in the limiting membranes of the endosomes has been shown to signal for apoptosis [45]. Whether EGFR signals for apoptosis or cell survival depends on the receptor location (spatial regulation of EGFR signaling) [46]–[48], rate of endocytosis and receptor trafficking (temporal regulation of EGFR signaling) [49], [50], and receptor clustering [51], [52].

Thus, by modulating EGFR signaling spatiotemporally or by modulating EGFR cell surface distribution and clustering, we might be able to switch the signal from growth to apoptosis.

1.5.3 Nanoconjugattion can modulate EGFR signaling

Conjugation of EGF to NPs has been shown to modulate EGFR signaling. L. Wu et al showed that nanoconjugated EGF[8] enhances EGF-induced apoptosis in EGFR overexpressing A431 cells [53]. They further studied the effect of nanoconjugated EGF in prolonging EGFR endosomal signaling by slowing down its endosomal trafficking pathway [54]. The fact that nanoconjugated ligands can exhibit a completely different and even opposite effect compared to their surface-loaded ligands in the free form, indicates the need for more fundamental studies about how NPs and their physicochemical properties such as size, shape, surface charge, and surface ligand density can modulate cellular processes.

[8] Conjugation of EGF with nanoparticles

1.6 Effect of NPs physicochemical properties on NP-cell interactions

When designing NP-based therapeutics, the first thing that must be taken into consideration is how NPs interact with the biological entities and target cells, which depends on NP physicochemical properties. The first important properties of a biomaterial are biocompatibility and/or biodegradability. In case of NPs, other properties such as size, shape, surface charge, type of surface ligand and its density are also of great significance, due to nano-scale properties of materials, in order to enhance efficacy and reduce toxicity. If delivery is the aim, NP surface must be engineered in a way to reduce NP induced immune response and undesired protein corona formation, and to increase circulation time. NP physical properties such as size and shape must be designed to have optimum cargo loading, release, and cellular uptake simultaneously. Bellow, most important physicochemical properties of NPs are introduced.

1.6.1 NP size

Size of NPs plays a crucial role in modulating cellular processes. A lot of studies has been done to study the effect of NP size on cellular processes such as endocytic mechanisms [55]–[57], uptake efficiency [58], signaling pathways, apoptosis [59]–[61] etc. Several studies have shown that 50 nm spherical NPs show the highest uptake rate [55], [62]–[64]. Different NP sizes are also endocytosed via different endocytic pathways. Size of NPs endocytosed by clathrin-mediated pits has been reported to be <200 nm whereas NPs above 200 nm start to be internalized via caveolae mediated endocytosis

which becomes predominant for NPs with about 500 nm in size [65], [66]. Fig 4 shows a schematic of different endocytic pathways of NPs known so far.

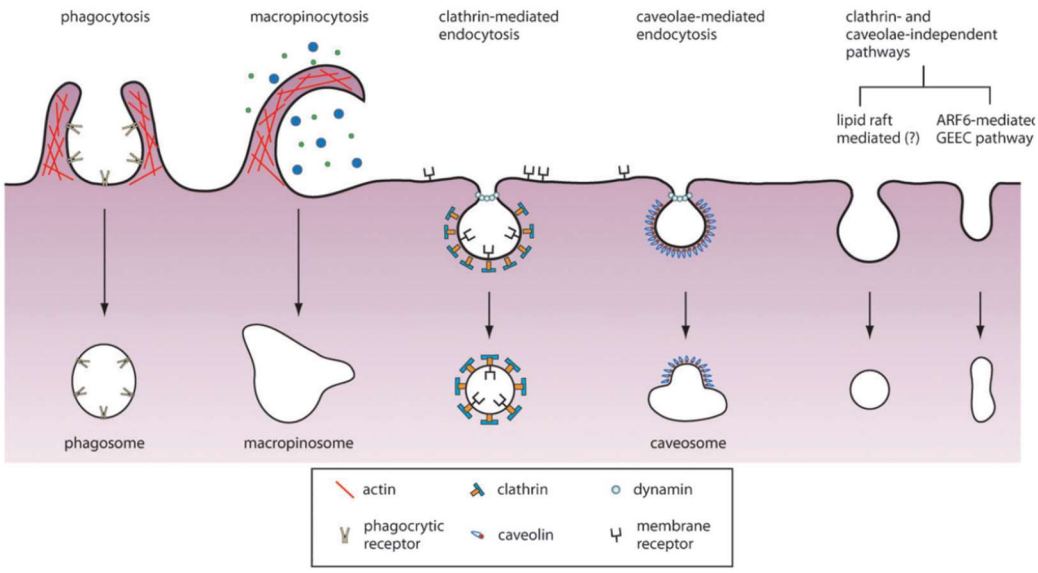

Fig. 1-4 Schematic of endocytic pathways [28].[9]

1.6.2 NP surface ligand density

NP surface ligand density also plays an important role in cellular uptake efficiency. D.R. Elias et al, showed that 50 nm NPs show significantly different uptake rate based on their surface ligand density. In fact, similar to size, there is an optimum ligand density which leads to the highest uptake efficiency [51], [67]. Therefore, when describing a NPs behavior in terms of cellular uptake efficiency, surface ligand density should be also considered since it may shift the optimum NP size for higher uptake efficiency.

[9] Reprinted from publication title "Strategies for the intracellular delivery of nanoparticles," vol. 40, no. 1, pp. 233–245, 2011, L. Y. T. Chou, K. Ming, and W. C. W. Chan, Chem. Soc. Rev., copyright (2011).

Significance of surface ligand density further emerges when the aim is studying or utilizing active targeting of NPs indicating the importance of optimizing NPs based on not only size but also ligand surface density to obtain the most efficient and desired modulation of cellular processes such as cell uptake for delivery applications or modulation of cell signaling pathways for therapeutic applications.

1.6.3 NP shape

NPs can be synthesized in a variety of shapes such as spheres, rods, stars, tubes, triangles, etc. Cells also behave differently when they interact with NPs with different shapes. Long nanorods and NPs with sharp edges has been shown to have higher binding and cellular uptake rate [21], [68]. However, they can induce a higher cytotoxicity compared to nanospheres, which is also cell type dependent [69].

An important point to consider when studying the effect of NP physicochemical properties on cell-NP interaction is the fact of contribution of several NP physicochemical factors in the overall cellular response to NPs. Cell type, cell media, type of experiment (in vitro/in vivo), NP concentration, size, shape, NP surface ligand type and density, all influence the way cells interact with NPs. This may cause different studies appear to have contradictory results. In conclusion, it is difficult to generalize a single NP property with a specific cell response and still more detailed and in-depth studies on NP-cell interactions are required and NP design must be optimized based on the desired, specific application.

1.7 NPs and cell signaling pathways

1.7.1 What is cell signaling

"Cell signaling refers to the vast networks of communication that occur between and within each cell in our body. Unlike the stable bricks that lay the foundation of our houses, cells are dynamic and ever-active building blocks. In effect, cell signaling makes this possible."[10] Here, the intracellular communication system aspect of cell signaling is our focus. The three stages of cell signaling are:

1. Reception, the stage when signal molecule binds a cell surface receptor
2. Signal transduction, the stage when the signal initiates a series of enzymatic reactions called signal transduction cascade.
3. Response, which is the cellular response such as cell growth, proliferation, differentiation, migration, or apoptosis.

Due to their nanometer-scale properties, NPs can initiate cell signaling pathways or, in case of nano-conjugation, even a different cell signaling pathway compared to their surface ligand or loaded cargo. The significance of studying NP-induced/enhanced cell signaling pathways arises, when therapeutic application of NPs is the aim in order to design highly efficient and effective NPs with minimal undesired side effects and capability of initiating or enhancing desired cell signaling pathways.

[10] https://biologydictionary.net/cell-signaling/

1.7.2 NP-induced/enhanced generation of reactive oxygen species (ROS), nitric oxide (NO)

1.7.2.1 What are ROS and NO?

Reactive oxygen species are chemically reactive species which contain oxygen. ROS are produced by NADPH oxidases enzymatic activity whereas NO is produced by enzymatic activity of nitric oxide synthases (NOS). Peroxides, superoxides, hydroxyl radicals, singlet oxygen, and alpha-oxygen are ROS.

1.7.2.2 ROS and NO as second messengers in cancer

ROS and NO have been proved to act as second messengers [70]–[73], i.e. intracellular signaling molecules that can trigger cell survival or apoptosis signals in response to extracellular signaling molecules. ROS/NO have been shown to signal for cell survival or apoptosis dependent of their intracellular levels. When low ROS levels has been shown to effectively regulate mitosis, cell growth, proliferation and angiogenesis in cancer, high ROS levels are linked with toxicity in cancer cells [74], [75]. Figure 5 shows how ROS regulates cellular processes. As shown in the figure, moderate ROS levels promote tumorigenesis whereas high levels are toxic to cancer cells.

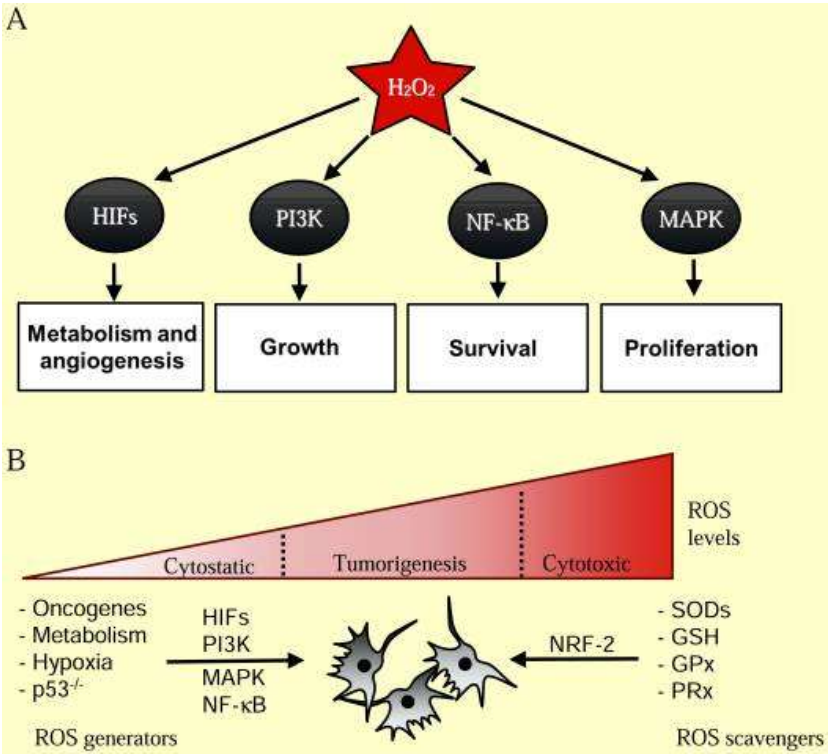

Fig. 1-5 ROS signaling is dose-dependent [75].[11]

Similar to ROS, NO has also a dual role in cancer which is concentration dependent [76]–[78] (figure 1-6).

[11] Reprinted from publication title "ROS Function in Redox Signaling and Oxidative Stress Michael," vol. 24, no. 10, pp. 1–25, 2015. A. Manuscript and O. Stress, Curr Biol. copyright (2015).

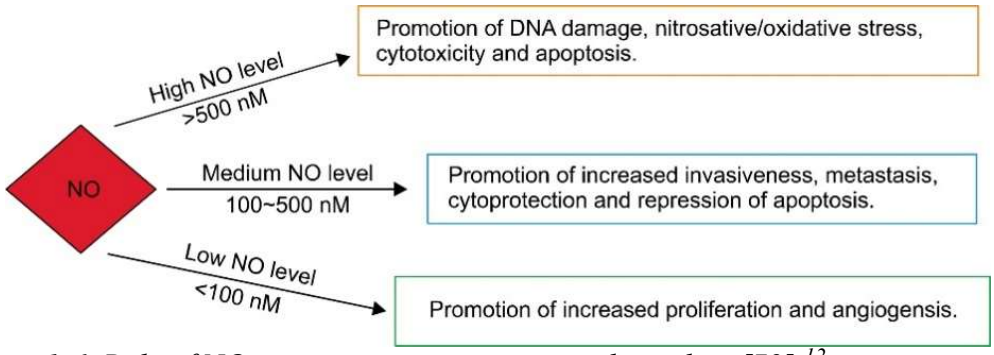

Fig. 1-6. Role of NO in cancer is concentration-dependent [79].[12]

1.7.2.3 Mechanism of ROS and NO signal initiation

Mechanism of ROS redox signaling involves oxidation of cysteine residues within proteins. "Cysteine residues exist as a thiolate anion ($Cys\text{-}S^-$) at physiological pH and are more susceptible to oxidation compared to the protonated cysteine thiol (Cys-SH). During redox signaling, H_2O_2 oxidizes the thiolate anion to sulfenic form (Cys-SOH) causing allosteric changes within the protein that alters its function." [75]. ROS has been shown to activate MAPK and ERK signaling pathways [80]. Figure 7 shows major ROS signaling pathways.

NO signaling activity derives from its redox reactivity and nitrosylation of thiols in enzymes such as kinases, caspases, etc [81]–[84]. NO has also been linked to activating oncogenic pathways, and EGFR signaling and stimulating tumorigenesis [82].

[12] Reprinted from publication title "The Potential Role of Nitric Oxide in Halting Cancer Progression Through Chemoprevention," vol. 21, no. 1, pp. 1–12, H. Vahora, M. A. Khan, U. Alalami, and A. Hussain, J. Cancer Prev. copyright (2016)

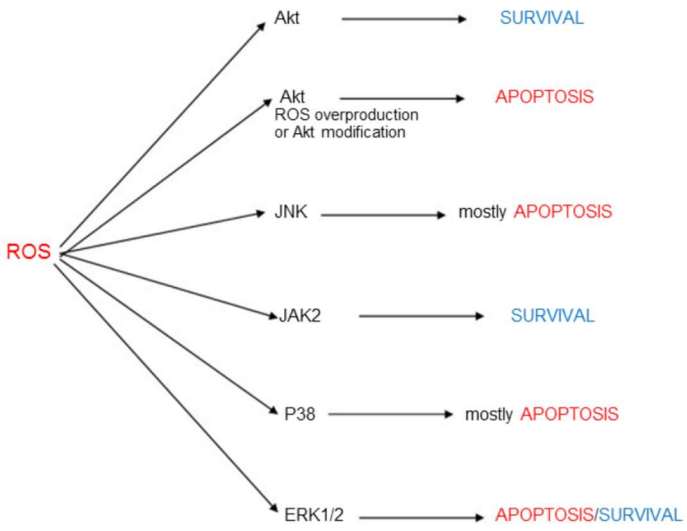

Fig. 1-7. ROS signaling pathways in cancer [85].[13]

1.7.2.4 EGFR-mediated generation of ROS/NO

EGFR signaling is important in understanding tumor progression due to its vital role in signaling for cell survival and tumor progression. Therefore, understanding the interplay between EGFR and ROS signaling is required for understanding mechanism of tumor progression [86]. It has been shown that EGFR activation can result in localized generation of H_2O_2 through NADPH oxidases. Generated ROS can modify specific cysteine residues in the EGFR active site leading to activation of intracellular signaling cascades [86]. EGF has also been shown to activate NOS and NO generation through EGFR signaling [77], [87]. The role of NPs in enhancing EGF-induced ROS has not been studied before.

[13] Reprinted from publication title "Reactive oxygen species signaling in cancer: comparison with aging.," vol. 2, no. 3, pp. 219–30, 2011. I. Afanas'ev, *Aging Dis.*, copyright (2011).

Considering the role of ROS as an important signaling molecule it is important to understand how NPs modulate ROS generation and signaling.

1.8 NPs and enhancing drug potency

It has been shown that combination of drugs and NPs can synergistically enhance the efficacy of drugs. Y. G. Yuan et al showed that silver NPs can enhance apoptotic efficacy of gemcitabine in human ovarian cancer cells [88]. It can be an evidence that in addition to the capability of NPs to deliver cargo more efficiently to the target cells, NPs may exhibit new properties in enhancing cargo efficacy which is not necessarily due to delivering more cargo. This *Potential role of NPs as not only drug carriers but also* ***enhancing drug efficacy*** *is intriguing and proposes not only new NP-based approaches for therapeutics but also may reveal novel properties of NPs in this context, that needs to be further studied.*

1.9 Aim and significance

Despite the existence of many studies in the area of NP-cell interactions, there is still a need for more detailed and specific study of how NPs with different physicochemical properties interact with cells, and the mechanism of interaction to find optimum NP properties for improving therapeutic and drug delivery applications. Here, we worked on effect of NP physicochemical properties on NP-cell interactions in order to design a NP platform for enhancing delivery and efficacy in inducing death in cancer cells. To gain a

better understanding of NP-cell interaction, we also studied apoptotic signaling pathways mediated by our designed NPs. Our study can be classified into the following categories:

- Nanoparticle-cell interactions induced apoptosis: a case study with nanoconjugated epidermal growth factor

  Epidermal Growth Factor Presenting Polymer Nanoparticles Stimulate Nitric Oxide Generation and Modulate Apoptotic Signaling through Nitrosylation of JNK

2 Chapter 2

Nanoparticle–cell interactions induced apoptosis: a case study with nanoconjugated epidermal growth factor

1.1 Introduction

The epidermal growth factor (EGF) receptor (EGFR) is a transmembrane receptor and a model receptor tyrosine kinase (RTK). EGFR is rapidly endocytosed after activation through ligand binding and subsequent dimerization.[1] EGFR signaling is key for healthy cell growth and differentiation, but EGFR overexpression or dysregulation is associated with uncontrolled cell growth and cancer.[2,3] The medical relevance of EGFR is, however, not limited to cancer. This receptor is also important for regulating neural plasticity[4,5] and intestinal barrier function,[6] and represents a therapeutic target in Alzheimer's disease.[7] Intriguingly, EGFR signaling can, under specific conditions, also block proliferation and initiate a programmed cell death (apoptosis) pathway.[8–10]There is now mounting evidence that this apparent contradiction results from a perturbation of the spatial regulation of EGFR signaling. Although EGFR is activated through ligand binding at the cell surface, activated EGFR signaling continues after uptake until the EGFR containing endosome having the phosphorylated EGFR tail exposed in the cytoplasm is enclosed in a multivesicular body, or the EGF-EGFR complex is degraded. In the case of free EGF it was hypothesized that the signaling outcome can vary with the cellular location of signaling.[11] Indeed, accumulation of activated EGFR in the limiting membrane of early endosomes was shown to trigger apoptosis.[12–15]

EGF-EGFR recognition is utilized to target cancer cells for diagnostic and therapeutic purposes with NP.[16–19] The rational development of optimized targeting strategies requires a detailed understanding of NP–cell interactions during and after uptake.[20–24] A particularly important question for a ligand–receptor pair, such as EGF-EGFR, whose signaling is potentially spatially regulated, is whether nanoconjugation of the ligand and its consequences

on uptake and intracellular trafficking impact the signaling outcome and whether this effect by itself has therapeutic potential. Indeed, recent studies have found that conjugation of EGF to gold NP results in apoptosis, as evidenced by increased caspase-3 levels, nucleus condensation, and Annexin V/propidium ion staining patterns, at a much lower concentration than observed for the free ligand.[25] The gain in apoptotic efficacy due to the nanoconjugation of EGF was confirmed in both EGFR overexpressors (A431, MDA-MB-468) as well as in cells with physiological EGFR expression levels (HeLa).[25,26] The mechanism by which nanoconjugation of EGF "switches" the signaling outcome from proliferation to apoptosis and how the effect depends on the physico-chemical properties of the NP core remain, however, unclear. As an important first step towards an improved understanding of the underlying NP–cell interactions that modulate EGF signaling, we characterize in this work the dependence of NP-EGF induced apoptosis on the intrinsic NP parameters size, shape, and EGF surface loading and elucidate the role of NP-EGF induced oxidative stress in inducing apoptosis.

2.1 Experimental

2.1.1 NP functionalization with EGF

100 µL of 10 mM PEG1 ($HS–(CH_2)_{11}–(C_2H_4O)_6–COOH$) and 10 µL of 10 mM PEG2 ($HS–CH_2CH_2–(C_2H_4O)_{77}–N_3$) solutions were added to 20 mL of gold nanosphere colloids and incubated overnight at room temperature. The particles were then washed twice by centrifugation and resuspension in millipore water. Subsequently, 2 µL of a 100 mg mL^{-1} propargyl-*N*-hydroxysuccinimidyl ester ($C_{10}H_{11}NO_5$) solution in DMSO were added to 100 µL of a 1 mg mL^{-1} solution of EGF in 1× PBS, pH 7.4, and incubated on ice for 6 h. This mixture was then dialyzed against 0.5× PBS for 72 h. 5 µL of the obtained propargyl-PEG-EGF

(concentration 10 nM) were then incubated overnight at 4 °C with 1 mL of the PEGylated gold nanospheres in the presence of 500 μM ascorbic acid and 100 μM $CuSO_4$ (catalyst for the cycloaddition reaction). The resulting EGF-functionalized particles (NP-EGF) were washed by centrifugation (2×) and resuspended in 1 mL of DMEM.

2.1.2 NR pegylation and functionalization with EGF

2.5 μL of 10 mM solutions of PEG1 and PEG2 were added to 1 mL of Au NR colloid (concentration = 100 pM) in the presence of 3% v/v of Tween 20 and subsequently incubated under soft stirring overnight at room temperature. The PEGylated Au NRs were washed twice by centrifugation (7500–15 000 rpm, 15 min–40 min depending on the NP dimensions) and resuspended in millipore water. 2 μL of a 100 mg mL^{-1} propargyl-PEG-NHS ester solution in DMSO were added to 100 μL of a 1 mg mL^{-1}solution of EGF in 1× PBS, pH 7.4, and incubated in an ice bath for 6 h. This mixture was then dialyzed against 0.5× PBS for 72 h with a 3.5 kDa molecular weight membrane. 10 μL of the obtained propargyl-PEG-EGF were incubated overnight at 4 °C with 1 mL of PEGylated Au NR colloid containing 500 μM ascorbic acid and 100 μM $CuSO_4$ as the catalyzer for the cycloaddition reaction. The resulting EGF-functionalized rods (NR-EGF) were washed 2× by centrifugation (7500–15 000 rpm, 15 min–40 min depending on the NR size). After that, NR-EGF was resuspended in 1 mL DMEM.

2.1.3 Caspase-3 activity and quantification of apoptosis enhancement

MDA-MB-468 cells were plated in 6-well dishes. After ≈80% cell confluency was reached the growth medium was replaced by fresh medium containing NP or free EGF ligand controls. The cells were incubated with the NP preparations for 4 h and then washed three times with Hank's

buffer. After that the cells were further incubated in growth media for 20 h. Finally, the particles were trypsinized with 0.5 mL of a 0.25% trypsin–EDTA solution. The trypsinization was quenched after 5 min by adding 0.5 mL of complete medium in each well. The cells were collected by centrifugation (300*g*, 5 min) and washed once with 1× PBS. Subsequently, the cells were resuspended in 1× PBS (800 µL). The EnzChek® Caspase-3 assay was applied to determine apoptosis activity according to the manufacturer's protocol in a 96-well plate. Fluorescence was quantified with a PerkinElmer 1420 Victor-3 multi-label counter using excitation and emission wavelengths of λ_{exc} = 485 nm and λ_{em} = 535 nm, respectively. The apoptosis enhancement was calculated from the measured caspase-3 levels as the change in apoptosis relative to the no treatment control. All caspase-3 activities were normalized by the total protein concentration determined by a BCA assay to account for the differences in sample size.

2.1.4 ROS quantification

Flow cytometry was used to quantify ROS generation. Cytoplasmic ROS generation was quantified using the CellROX deep red flow cytometry assay kit (Invitrogen, C10422). 1 mM *N*-acetylcysteine (NAC) was used as an antioxidant to suppress ROS generation and 200 µM *tert*-butyl hydroperoxide (TBHP) was used as a positive control to induce ROS. Mitochondrial superoxide levels were quantified with a MitoSOX Red Mitochondrial Superoxide Indicator (Invitrogen, M36008). This compound is a hydroethidine derivative that selectively localizes to the mitochondria.

2.1.5 GSH quantification

Cellular GSH levels were measured with the GSH/GSSG ratio detection assay kit (Fluorimetric-Green) following the manufacturer's protocol (Abcam, ab138881). GSH levels were evaluated after incubation for 4 h with $NP_{78.9}$-EGF.

2.1.6 Mitochondrial membrane potential assay

The cells were cultured in 6-well dishes. 20 μM tetraethylbenzimidazolylcarbocyanine (JC1) was added to the control and sample wells and incubated for 10 min at 37 °C. The wells were washed with Hank's buffer (HBSS) twice before $NP_{78.9}$-EGF was added and incubated for 4 h. 4 μl of carbonyl cyanide 4-(trifluoromethoxy) phenylhydrazone (FCCP) was included as a positive control. The cells were detached, washed with PBS and then analyzed through flow cytometry with an emission wavelength of 590 nm.

2.1.7 ICP-MS quantification of cellular NP uptake

MDA-MB-468 cells were plated in 6-well dishes. After 24 h, the old growth medium was replaced with a fresh medium containing nanoconjugated EGF, with the NP-EGF concentration varying depending on the NP core size between 8–128 pM, or PEGylated NP at a concentration of 100 pM for 4 h and then washed three times with Hank's buffer. After that the cells were further incubated in growth media for 20 h before they were trypsinized with 1 mL of 0.25% trypsin-EDTA solution and subsequent quenching of the enzyme by the addition of 1 mL of complete medium in each well. The cells were collected by centrifugation (200*g*, 5 min) and subsequently washed twice with 1× PBS. The cell densities of the samples were determined through a hemacytometer (no less than 200 cells). Aqua regia (1 mL) was added to the cells in

a total volume of 10 μL to dissolve the Au NP. The mixture was then dried overnight at 65 °C and re-dissolved in HCl solution (1 mL, 2%). After an additional 4-fold dilution through millipore water, the samples were inserted into a VG Plasma Quad ExCell ICP-MS. For etching control experiments an additional step was performed before trypsinization. 1 mL of the I_2/KI aqueous solution (0.34 mM I_2, 2.04 mM KI in PBS) was added to the culture well and incubated at room temperature for 2 min and then washed 3 times with pre-warmed Hank's buffer.

2.1.8 Quantification of EGFR phosphorylation

NP-EGF was incubated with MDA-MB-468 cells in DMEM for defined time durations. The cells were washed in Hank's buffer to remove the particles and then detached and lysed. The lysate was diluted 10× before the phosphorylation levels were measured using a phosphorylated human EGFR (pY1068) Elisa kit following the manufacturer's directions.

2.2 Results

2.2.1 Apoptosis enhancement through spherical NP-EGF and the effect of NP size

The design of NP-EGF used in this study is schematically depicted in Fig. 1a. The NP surface was passivated with a self-assembled monolayer of (HS–$(CH_2)_{11}$–$(C_2H_4O)_6$–COOH, PEG1) interspersed with (HS–CH_2CH_2–$(C_2H_4O)_{77}$–N_3, PEG2) for the covalent attachment of alkyne functionalized EGF through the Cu^I catalyzed 1,3-dipolar cycloaddition reaction.[27,28] We included three spherical NP sizes in the size range between 1–100 nm: 21.5 ± 0.9 nm ($NP_{21.5}$), 40.4 ± 1.0 nm ($NP_{40.4}$), and 78.9 ± 1.3 nm ($NP_{78.9}$). In the initial test experiments we also tested 98.1 ± 0.8 ($NP_{98.1}$) particles, but these larger NP lacked sufficient stability when incubated with the cells and resulted in unacceptable levels of agglomeration (Fig. 2-1).

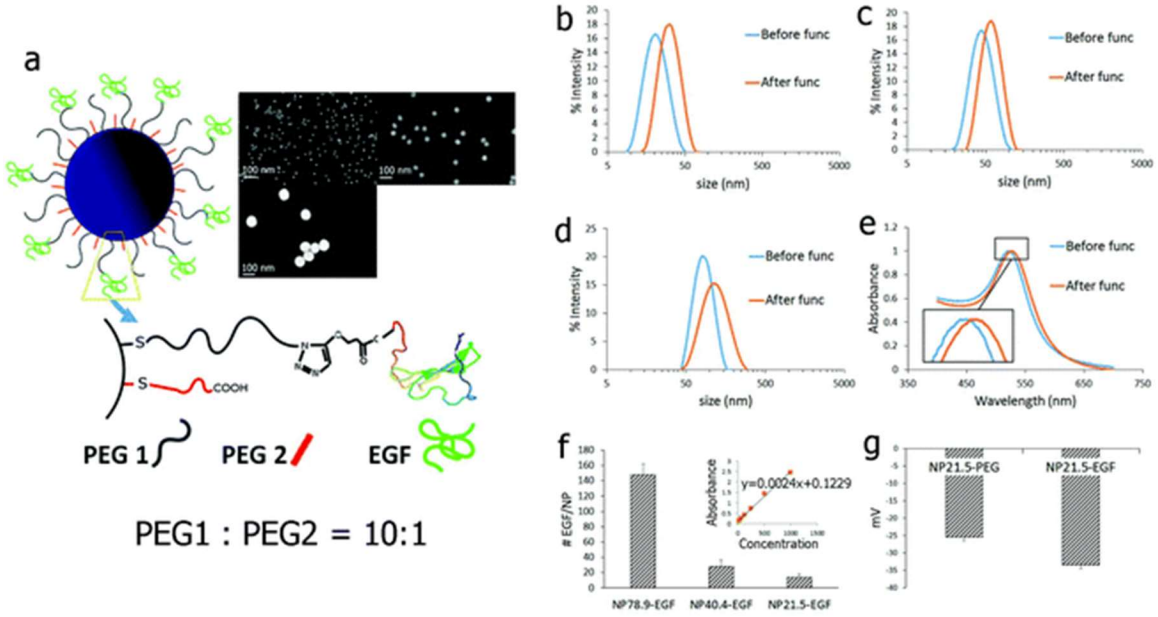

Fig. 2-1(a) Schematic drawing of the NP-EGF used in this work. PEG1 = HS–$(CH_2)_{11}$–$(C_2H_4O)_6$–COOH; PEG2 = HS–CH_2CH_2–$(C_2H_4O)_{77}$–N_3. The inset shows SEM images of the different NP cores used. The average NP size (± standard deviation) is (clockwise): 21.5 ± 0.9 nm; 40.4 ± 1.0 nm; 78.9 ± 1.3 nm. (b)–(d) Hydrodynamic diameter (intensity statistics) as determined by DLS of citrate capped (b) $NP_{21.5}$, (c) $NP_{40.4}$, and (d) $NP_{78.9}$. (e) UV-Vis for $NP_{40.4}$ before and after functionalization with EGF. (f) Number of EGF bound per NP for (left to right): $NP_{78.9}$-EGF, $NP_{40.4}$-EGF, $NP_{21.5}$-EGF. Inset shows ELISA calibration standard obtained with free EGF. (g) Zeta-potentials of $NP_{21.5}$ before ($NP_{21.5}$-PEG) and after ($NP_{21.5}$-EGF) functionalization with EGF.

The SEM images of the NP cores and size distributions as determined by dynamic light scattering (DLS, intensity statistics) for NP and NP-EGF are summarized in Fig. 2-1a–d. Fig.

1e contains UV-Vis spectra for $NP_{40.4}$ before and after functionalization with EGF. A small systematic red-shift of about 5 nm indicates a change in the local refractive index due to a successful loading of the NP with EGF.[29,30] The number of EGF ligands per NP was determined by ELISA (Fig. 1f). We found that on average 14, 30, 150 EGF were bound to the different NP diameters (in the order of increasing diameter), corresponding to an average EGF surface density of $(8.17 \pm 2.64) \times 10^3\ \mu m^{-2}$. The zeta-potential increase obtained after cross-linking (Fig. 1g) further confirms a successful functionalization of the NP cores with EGF.

Previous studies have shown that EGF nanoconjugation triggers apoptosis in different cancer cell lines (A431, MDA-MB-468, HeLa).[25,26] In this study, we focus on the EGFR-overexpressing MDA-MB-468 breast cancer cell line, which is an established model system for investigating the apoptotic efficacy of free EGF.[14] We chose a relatively short incubation time of 4 h for NP-EGF with the cells in our studies to provide a stringent test of the efficacy of NP-EGF with different NP core diameters and shapes and to minimize the detrimental effects of long colloidal NP incubation times (agglomeration, NP settlement, non-specific binding, *etc*.). The NP were incubated in serum-free DMEM to minimize the corona[21,31–33] formation around the NP. After 4 h, the NP-EGF containing DMEM was removed and exchanged with fresh culture medium. The NP were then incubated for another 20 h before apoptosis was quantified by measuring the activity of the activated death protease caspase-3,[34,35] which plays a central role in the execution of both extrinsic and intrinsic apoptosis.[36] The apoptosis enhancement in % was calculated from the measured caspase-3 levels ([*Casp*]) of NP-EGF treated cells and untreated control as $100 \times ([Casp(\text{treated})] - [Casp(\text{control})])/[Casp(\text{control})]$.

When characterizing the impact of NP size on NP-EGF induced apoptosis, one needs to account for the differences in surface area, and thus the total EGF concentration, for the investigated NP diameters. In our experiments we adjusted the NP concentration to keep the effective EGF concentration constant at approximately 1.0 nM. We chose this concentration as it lies significantly below the threshold required for apoptosis induction by free EGF ligand. Unless otherwise noted, we used the following NP concentrations: 128.0 pM ($NP_{21.5}$), 32.0 pM ($NP_{40.4}$), and 8.0 pM ($NP_{78.9}$). The stability of NP-EGF under the chosen experimental conditions was assayed by UV-Vis and dynamic light scattering (Fig. S2 and S3†). Only $NP_{21.5}$-EGF showed some minor self-association, presumably due to the higher particle concentration in this case. However, as the contribution from agglomerates was low even in the case of $NP_{21.5}$-EGF, all NP preparations were used as prepared.

In Fig. 2a we summarize the measured apoptosis enhancement (relative to the untreated control) for spherical NP-EGF with the investigated core diameters and for the following controls: 1 nM and 40 nM free EGF and the supernatant of the last wash for $NP_{78.9}$-EGF. We also performed apoptosis measurements for pegylated NP ($NP_{21.5}$-PEG, $NP_{40.4}$-PEG, $NP_{78.9}$-PEG) that did not contain any EGF (Fig. 2b). None of the different NP-PEG samples, the free EGF samples, or the last wash show any significant apoptosis enhancement. This is different for nanoconjugated EGF. $NP_{78.9}$-EGF achieves a significant ($p < 0.0001$) increase in the average apoptosis enhancement (up to approx. 40%), whereas conjugates with a smaller NP core ($NP_{21.5}$-EGF and $NP_{40.4}$-EGF) failed to induce apoptosis (no significant change) if the NP exposure was limited to 4 h. When comparing the apoptosis levels measured for one effective EGF concentration with different NP sizes, the peptide concentration bound to a NP is not

necessarily equivalent to that of the free peptide, as all of the peptides bound to one NP effectively interact with one or a few receptors to which the NP is bound. We emphasize, however, that this effect further increases the "effective" EGF concentration of the smaller NP when compared with $NP_{78.9}$-EGF, making the apoptosis enhancement for $NP_{78.9}$ even more significant. In fact, even greatly increased concentrations of smaller NP-EGF with diameters <78.9 nm did not achieve comparable apoptosis levels as observed for 8.0 pM $NP_{78.9}$-EGF (*vide infra*).

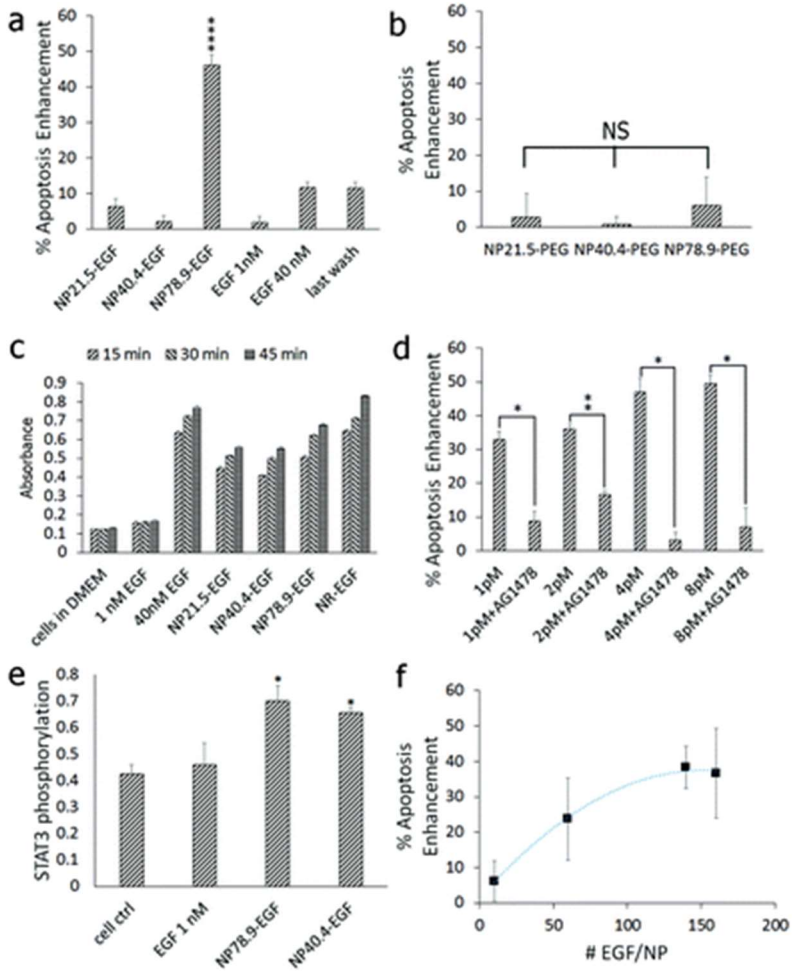

*Fig. 2-2 (a) Caspase-3 activity (relative to the untreated control) measured after 4 h of exposure to (from left to right) $NP_{21.5}$-EGF, $NP_{40.4}$-EGF, $NP_{78.9}$-EGF, $NP_{98.1}$-EGF, 1 nM free EGF, 40 nM free EGF, and the supernatant of the last wash of $NP_{98.1}$-EGF. The effective EGF concentration for the different NP-EGF concentrations was 1.0 nM (see text). The plotted data were collected in at least six independent experiments. Error bars show standard errors of the mean. Only $NP_{78.9}$-EGF show a significant increase at a significance level of ****$p < 0.0001$. (b) Caspase-3 activity (relative to the untreated control) for pegylated NP (no EGF) as a function of NP core size. NS = not significant. (c)*

*ELISA absorbance signal of phosphorylated EGFR after 15, 30, and 45 min of incubation with (from left to right): untreated control, 1 nM free EGF, 40 nM free EGF, $NP_{21.5}$-EGF, $NP_{40.4}$-EGF, $NP_{78.9}$-EGF, NR-EGF (AR = 8.6). (d) Apoptosis enhancement as a function of $NP_{78.9}$-EGF concentration in the absence and presence of the RTK inhibitor AG1478 (250 nM). The effective EGF concentrations are 0.15 nM, 0.30 nM, 0.60 nM, and 1.20 nM. *$p < 0.05$, **$p < 0.01$. (e) STAT3 phosphorylation for untreated control, 1 nM free EGF, and $NP_{78.9}$-EGF and $NP_{40.4}$-EGF with an effective EGF concentration of 1 nM (*$p < 0.05$ relative to the cell control). (f) Apoptosis enhancement as a function of number of EGF peptides bound to $NP_{78.9}$-EGF. Data in (b) and (f) were collected in three independent experiments; data in (c)–(e) were collected from two independent experiments. Error bars show standard deviations.*

We measured the average EGFR activation as global phosphorylation for $NP_{21.5}$-EGF, $NP_{40.4}$-EGF, $NP_{78.9}$-EGF, EGF-conjugated nanorods (NR-EGF) with an aspect ratio of AR = 8.6, as well as for 1 nM and 40 nM free EGF, and the untreated control 15, 30, and 45 min after addition of EGF or its nanoconjugate. The measured phosphorylation levels (Fig. 2c) confirm that all EGF nanoconjugates retain the ability to activate EGFR. For $NP_{78.9}$-EGF, we also evaluated EGFR phosphorylation in the presence and absence of an EGFR-selective RTK inhibitor (AG1478). In the presence of the inhibitor we observed, as expected, a suppression of phosphorylation (Fig. S4†).

For $NP_{78.9}$-EGF we evaluated the apoptosis enhancement for different concentrations in the absence and presence of the EGFR-selective RTK inhibitor AG1478 (Fig. 2d). In the absence of the inhibitor we observed a systematic increase of apoptosis enhancement as a function of increasing concentrations, while the RTK inhibitor suppressed apoptosis for all $NP_{78.9}$-EGF concentrations. The significant difference between the experimental conditions ± AG1478 confirms that the observed apoptosis is EGFR-dependent.

The signal and transducer and activator of transcription 3 (STAT3) has been indicated to play a major role in initiating apoptosis in response to free EGF.[37] Indeed, we found significantly enhanced STAT3 phosphorylation levels for nanoconjugated EGF but not for free EGF (Fig. 2e) after 4 h of NP-EGF exposure, which is consistent with the overall higher apoptotic efficacy of NP-EGF when compared with free EGF. We did, however, not detect any significant difference in STAT3 activation between $NP_{40.4}$-EGF and $NP_{78.9}$-EGF although according to Fig. 2a the larger NP core has a higher apoptotic efficacy. This finding implies that STAT3 activation alone is insufficient to account for the differences observed for nanoconjugated EGF with different core sizes, confirming a NP-dependent modulation of the apoptotic efficacy of EGF.

2.2.2 Effect of EGF surface density on apoptosis enhancement

Another effect that modifies the apoptotic efficacy of nanoconjugated EGF is multivalency. Multivalent presentation of a ligand on a NP leads to increased binding avidities and can potentially impact the signaling outcomes. Indeed, we observed that the apoptosis enhancement increases with the growing EGF density on the NP. This is exemplified for $NP_{78.9}$-EGF with different EGF densities in Fig. 2f. The measured apoptosis initially increases with the number of bound EGF/NP but then converges. For the two highest EGF densities, 140 EGF/NP (≈7.0 ×

10^3 μm^{-2}) and 160 EGF/NP (≈8.0 × 10^3 μm^{-2}), no difference in apoptosis enhancement is detected. Unless otherwise noted, we used an average EGF surface density of (7.8 ± 2.3) × 10^3 μm^{-2} with EGF surface densities >6000 μm^{-2} for all NP sizes throughout this manuscript. The NP-EGF lies in the "high" EGF loading regime where the apoptosis enhancement is independent of the EGF surface concentration. To account for the potential differences in the NP uptake due to different binding affinities related to variations in the number of available EGF per particle as well as intrinsic size differences in the uptake mechanism itself, we next quantified the uptake of NP-EGF as a function of NP core size.

2.2.3 Size *versus* concentration effect

We first validated that the EGF bound to the NP is available and that the NP-EGF uptake is EGF-specific. Fig. 3a shows the dark-field scattering images of MDA-MB-468 cells after incubation with $NP_{78.9}$-EGF (left) and $NP_{78.9}$-PEG (right). Only the EGF-functionalized NP show a systematic binding, indicating that the observed binding is EGF-mediated. We quantified the uptake for the EGF- and PEG-functionalized NP of all core sizes by ICP-MS (Fig. 3b). For the 1 nM EGF preparations the number of NP per cell increases in the following order $NP_{78.9}$-EGF > $NP_{40.4}$-EGF > $NP_{21.5}$-EGF. For all investigated NP sizes the uptake of NP-EGF was higher than that of NP-PEG, confirming the receptor-mediated uptake of the nanoconjugated EGF for all NP sizes.[26] Selective removal of surface bound NP with mild KI/I_2 etching[38] under conditions that removed all solvent-accessible NP (Fig. S5†) revealed that even for the largest NP size at least 50% of the NP were protected from the etchant through internalization (labeled $NP_{78.9}$-EGF-etched in Fig. 3b).

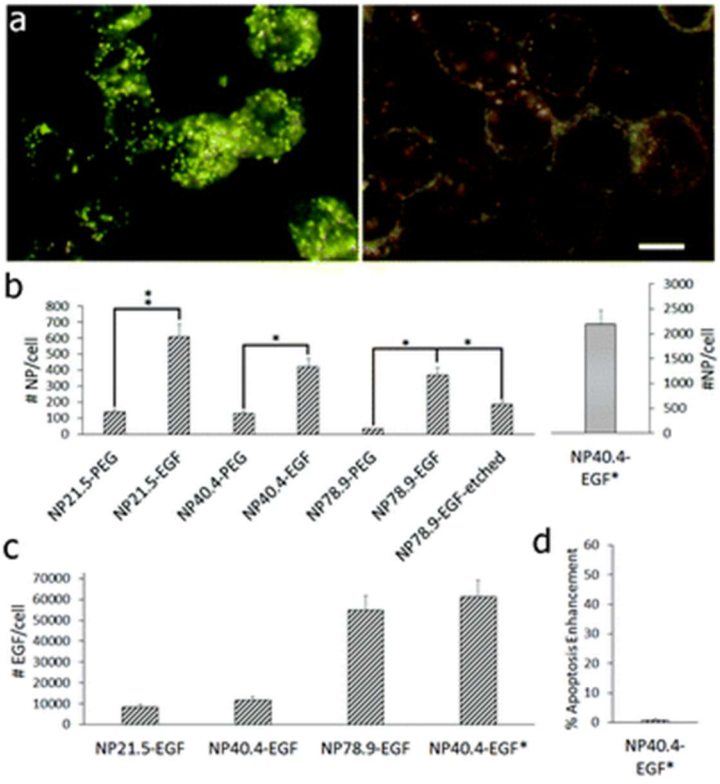

Fig. 2-3(a) Darkfield image of MDA-MB-468 cells after incubation with $NP_{78.9}$-EGF (left) and $NP_{78.9}$-PEG (right) under otherwise identical conditions. Scale bar is 10 μm. (b) Average number of particles uptake into MDA-MB-468 cells determined by ICP-MS for NP-PEG and NP-EGF with core diameters (left to right) of 21.5 nm, 40.4 nm, 78.9 nm. For the NP diameter of 78.9 nm we also included the data obtained after mild KI/I_2 etching that preferentially removes surface bound NP ("etched"). The effective EGF concentration for all conditions was 1 nM, except for $NP_{40.4}$-EGF, which contained an effective EGF concentration of 1.2 μM. *p < 0.05; **p < 0.01. (c) Average number of EGF molecules delivered per cell for (left to right): $NP_{21.5}$-EGF, $NP_{40.4}$-EGF, $NP_{78.9}$-EGF, $NP_{40.4}$-EGF*.*

(d) Apoptosis enhancement obtained for $NP_{40.4}$-EGF. Data in (b)–(d) were collected from at least two independent experiments.*

Fig. 3c summarizes the average number of EGF peptides delivered per cell for all NP-EGF conjugates with a constant effective EGF concentration of 1 nM. The numbers were generated by multiplying the number of delivered NP by the number of bound EGF. Although the number of NP taken up decrease with the increasing diameter, the number of delivered EGF molecules increases for the different NP cores in the order of $NP_{21.5} < NP_{40.4} < NP_{78.9}$ due to the large difference in the bound ligands per particle.

The stark differences in the number of EGF molecules delivered between different NP sizes raise the question whether the high apoptotic efficacy of $NP_{78.9}$-EGF is related to the physical size of the $NP_{78.9}$ core or whether the higher intracellular concentration of EGF is the dominating factor. To address this important question, we measured the apoptosis enhancement for a smaller NP core at a greatly increased concentration. We used 400 nM $NP_{40.4}$-EGF (effective EGF concentration 1.2 μM) under otherwise identical conditions as before and obtained significantly higher NP uptake (included as $NP_{40.4}$-EGF* in Fig. 3b). The average number of EGF delivered per cell under these conditions (6.1×10^4 EGF per cell) was even higher than for $NP_{78.9}$-EGF (Fig. 3c). However, despite the strongly increased intracellular EGF concentration, $NP_{40.4}$-EGF still failed to result in a measurable apoptosis enhancement (Fig. 3d). This observation contradicts a simple EGF (or NP) concentration effect as a cause for the strong apoptosis of $NP_{78.9}$ and, instead, suggests an enhancement mechanism that is more sensitive to

the details of the nanoconjugation (size of the NP, ligand density, *etc*.) than to the number of delivered EGF. For instance, it is conceivable that the nanoconjugation has a crucial effect on the temporospatial regulation of EGFR signalling. Intriguingly, in cells exposed to free EGF, $NP_{21.5}$-EGF, or $NP_{78.9}$-EGF (effective EGF concentration was 1 nM in all cases) for 15 min and subsequently maintained in a serum-free medium for another 60 min before immunolabelling the early endosome marker EEA1, optical microscopy revealed a higher early endosome concentration for $NP_{78.9}$ than for $NP_{21.5}$ or free EGF (Fig. S6†). Considering that $NP_{21.5}$-EGF achieved comparable or higher intracellular NP concentrations than $NP_{78.9}$-EGF (Fig. 3b), this observation suggests that the $NP_{78.9}$ core triggers an accumulation of EGF in early endosomes, which is consistent with previous tracking studies that showed longer dwell times.[26]

2.2.4 NR-EGF fails to enhance apoptosis

In addition to size, shape is another physical NP property with potential relevance for determining the apoptotic efficacy of nanoconjugated EGF. To address the role of AR in EGF-mediated apoptosis enhancement we synthesized NR with average lengths (AR given in parenthesis) of 45.8 ± 5.5 nm (2.5), 60.9 ± 7.3 nm (3.6), 71.6 ± 9.6 nm (5.4), and 88.9 ± 11.0 nm (8.6) using the seed-mediated method described by Vigderman *et al.*[39] The anisotropic growth of NR was achieved with cetyltrimethylammonium bromide (CTAB) as a surface ligand. As this ligand is cytotoxic, we exchanged it against benign PEG in a postsynthetic step before EGF was introduced through a Cu^{I} catalyzed 1,3-dipolar cycloaddition reaction (Fig. 4a–c). SEM images and UV-Vis spectra of the NR used in this work are provided in Fig. 4d–g. Peak extinction wavelengths and zeta-potentials before/after PEGylation as well as the volumes and surface areas of the NR used in this work are summarized in Table S1.†

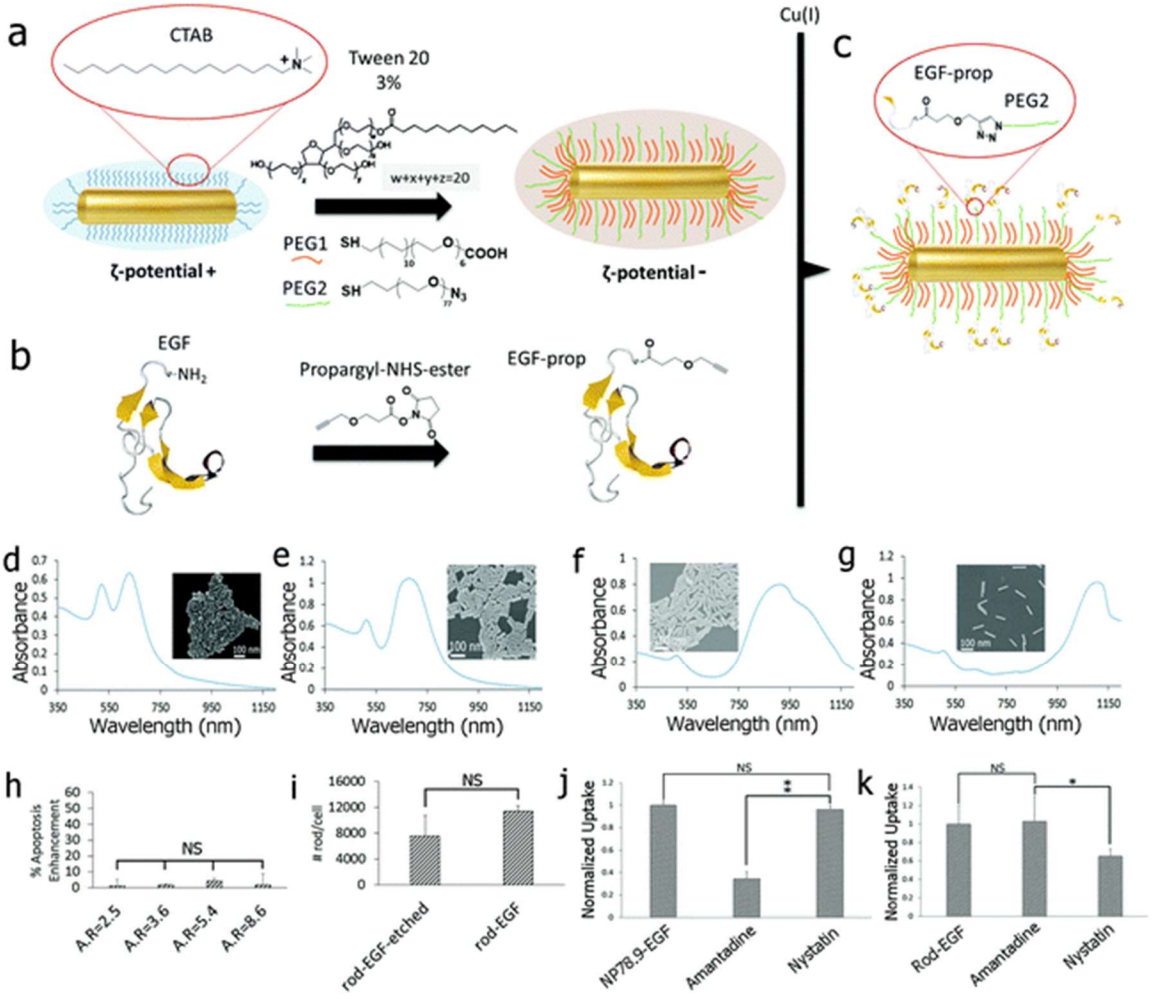

Fig. 2-4 (a) Gold NR were functionalized with PEG1 and PEG2 in the presence of 3% v/v of Tween 20 to stabilize the NP and to introduce the binding sites for EGF (see text). (b) Human EGF was modified with a terminal propargyl residue. (c) The modified EGF was tethered to the binding sites of the PEGylated NR through the Cu(I) catalyzed 1,3-dipolar cycloaddition reaction. (d)–(g) UV-Vis spectra and SEM images of the nanorods used in this work with AR = 2.5, 3.6, 5.4, 8.6. (h) Apoptosis enhancement measured for NR-EGF as function of AR under the same experimental conditions as for NP-EGF (1 nM effective

*EGF concentration, 4 h incubation with rods). (i) Average number of NR-EGF (AR = 8.6) per cell after (left) and before (right) KI/I_2etching. (j) Relative uptake of (left to right): $NP_{78.9}$-EGF, $NP_{78.9}$-EGF + amantadine, $NP_{78.9}$-EGF + nystatin into MDA-MB-468 determined by ICP-MS. (k) Cellular uptake of (left to right): NR-EGF (AR = 8.6), NR-EGF + amantadine, NR-EGF + nystatin. Data in (h)–(k) were collected from at least two independent experiments. Error bars show standard deviations. **p < 0.01; *p < 0.05; NS = not significant.*

The EGF loadings of the NR were in the order of increasing AR: 23, 58, 101, 160 EGF/NR. The average EGF density for all NR was $(2.7 \pm 2.0) \times 10^4$ μm^{-2}. Like before for the spherical NP, the NRs were incubated with NR-EGF corresponding to an effective EGF concentration of 1 nM. All experimental conditions were identical to the spherical NP-EGF studies (4 h incubation with NR, followed by 20 h incubation in serum containing medium), but none of the investigated AR led to a measurable enhancement in apoptosis (Fig. 4h). This is remarkable, considering (i) that the length of the two longest NRs is comparable to the diameter of $NP_{78.9}$ and (ii) that the number of bound EGF for the highest AR even slightly exceeds that of $NP_{78.9}$-EGF. Differences in the uptake behavior between NR and NP have recently attracted a lot of interest. It was observed that high AR NRs are taken up much more slowly than spherical NP.[40,41] We confirmed that the high AR NR-EGF used in this work were still taken up by comparing the cellular gold content before and after removing the solvent-accessible gold NR with KI/I_2 etchant through ICP-MS (Fig. 4i). The large fraction of protected NR observed in these

experiments confirms their intracellular uptake. However, the NR uptake, especially for high AR NR, does not necessarily occur along the same pathway as that of spherical NP.[42,43] This is relevant as shape-dependent differences in the uptake mechanisms can lead to different intracellular NP-EGF distributions.[44–46]

To verify the differences in the uptake of spherical $NP_{78.9}$-EGF and high AR NR-EGF (AR = 8.6), we performed uptake inhibition assays for clathrin- and caveolae-mediated endocytosis (Fig. 4j and k). We measured the cellular gold content though ICP-MS for the cells treated with nystatin as an inhibitor for caveolae-mediated endocytosis or amantadine as an inhibitor for clathrin-mediated endocytosis. The inhibition studies reveal that the $NP_{78.9}$-EGF uptake (Fig. 4j) is reduced through adamantine but not by nystatin, as expected for clathrin-mediated uptake. In contrast, for NR-EGF adamantine does not affect the uptake (Fig. 4k). Instead, we observe a reduction in uptake after nystatin treatment, indicative of caveolae-mediated endocytosis. Positive controls for the inhibitors are provided in Fig. S7.†

2.2.5 $NP_{78.9}$-EGF induced oxidative stress

Oxidative stress plays a central role in apoptosis, with relevance to both induction as well as execution. Although oxidative stress is often indicated in NP-induced apoptosis,[47–49] there are different mechanisms of ROS formation and the generated ROS can have different functions. Depending on the chemical composition of the NP and its ligands, NP and ligands may create ROS through redox reactions. Inert NP can trigger cellular responses that result in the ROS formation. For gold[50,51] and silver NP,[52,53]as well as for many metal–oxide NP,[54,55] ROS generation has been observed as a consequence of mitochondrial damage that results in apoptosis.[56] For the biofunctionalized NP, as for the NP investigated in this work, the

mechanism of ROS generation is furthermore expected to depend on the interplay between the ligand, NP, and cell receptor. Relevant in this context is that EGFR activation triggers ROS formation as signaling molecules, and H_2O_2, in particular, has been indicated in the receptor transactivation.[57–60]

As a first step towards a quantitative understanding of the relationship between EGF nanoconjugation and oxidative stress, we measured both cytoplasmic ROS and mitochondrial superoxide levels after the addition of $NP_{78.9}$-EGF. Fig. 5a summarizes the cytoplasmic ROS levels after $NP_{78.9}$-EGF incubation with MDA-MB-468 cells for 4 h, and Fig. 5b shows cytoplasmic ROS levels after maintaining the cells for an additional 20 h after removal of $NP_{78.9}$-EGF. Several controls were included: untreated, treatment with *tert*-butyl hydroperoxide (TBHP), and NP-EGF in the presence of NAC. Importantly, for both the investigated time points, $NP_{78.9}$-EGF was found to induce a strong increase in cytoplasmic ROS concentration that was almost identical to that obtained with the positive control, TBHP. The ROS levels for $NP_{78.9}$-EGF significantly exceeded those of free EGF at the same effective concentration (1 nM ligand). In Fig. 5b we also included the ROS levels for $NP_{78.9}$-PEG obtained under the otherwise identical conditions. The ROS levels for the latter were even lower than those of free EGF. The increased ROS levels for $NP_{78.9}$-EGF result from the synergistic interactions between the NP core and conjugated EGF.

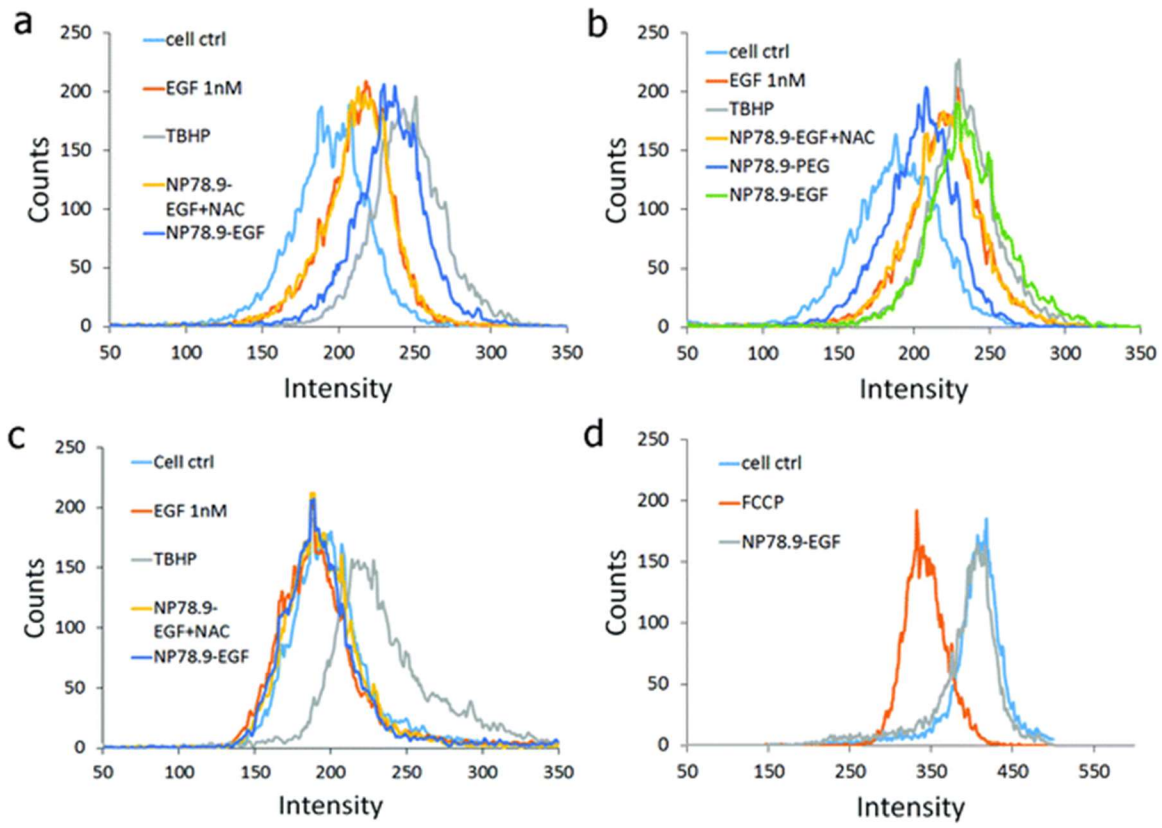

Fig. 2-5(a) Quantification of ROS levels through fluorescence flow cytometry using a CellRox assay. Fluorescence histogram for the untreated control, TBHP positive control, $NP_{78.9}$-EGF + NAC (NAC), and $NP_{78.9}$-EGF are included. (b) The same data as in (a) but after additional culturing for 20 h after removal of $NP_{78.9}$-EGF. $NP_{78.9}$-PEG was included as an additional control. (c) Quantification of mitochondrial ROS under the same conditions as in (a). (d) JC1 mitochondrial membrane potential assay. $NP_{78.9}$-EGF does not result in a measurable reduction in fluorescence intensity relative to the untreated control, indicating the intact mitochondrial membranes. FCCP = carbonyl cyanide 4-(trifluoromethoxy) phenylhydrazone is a positive control that reduces the mitochondrial potential.

We monitored the mitochondrial superoxide (O_2^-) concentration as the primary ROS generated in the mitochondria. Fig. 5cshows the mitochondrial superoxide concentrations for cells incubated for 4 h with $NP_{78.9}$-EGF and maintained for an additional 20 h in the incubator after the removal of $NP_{78.9}$-EGF as well as for the positive and negative controls. No significant increase in mitochondrial superoxide concentration was detected after $NP_{78.9}$-EGF treatment. We also did not detect any decrease in mitochondrial membrane potential (Fig. 5d). Overall, the data in Fig. 5a–d show that $NP_{78.9}$-EGF results in a significant increase in cytoplasmic ROS, but that the effect on mitochondrial ROS and membrane integrity is negligible.

2.2.6 $NP_{78.9}$-EGF impact on intracellular glutathione homeostasis and its effect on apoptosis

GSH is a major thiol-based redox buffer that in healthy cells is present in high concentrations in its reduced state and that is converted into its oxidized dimer state GSSG through reaction with ROS.[61,62] Importantly, the cellular GSH content is indicated to play a direct role in the induction and regulation of apoptosis.[63,64]Fig. 6a shows the cellular GSH/GSSG concentration ratio for $NP_{78.9}$-EGF, $NP_{40.4}$-EGF, $NP_{21.5}$-EGF, and $NP_{78.9}$-EGF in the presence of the EGFR-selective RTK inhibitor AG1478, and the anti-oxidants NAC (*N*-actylcysteine), trolox (6-hydroxy-2,5,7,8-tetramethylchroman-2-carboxylic acid), or tempol (4-hydroxy-2,2,6,6-tetramethylpiperidin-1-oxyl). In agreement with the size-dependence of the EGF nanoconjugation induced apoptosis, we found that the drop in GSH/GSSG ratio was specific to the $NP_{78.9}$ core; smaller NP cores did not induce a significant reduction in the GSH/GSSG ratio under the chosen experimental conditions. Importantly, the presence of the EGFR-specific RTK

inhibitor AG1478, or of the antioxidants NAC, trolox or tempol mitigated the oxidative stress induced by $NP_{78.9}$-EGF and prevented a significant drop in the GSH/GSSG ratio.

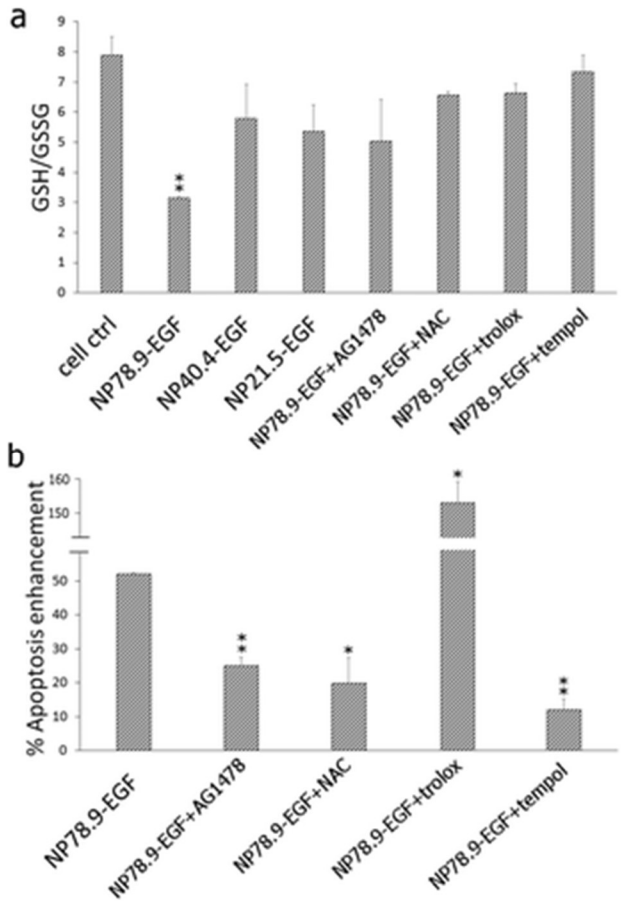

*Fig. 2-6(a) GSH/GSSG ratio for the untreated control, $NP_{78.9}$-EGF, $NP_{40.4}$-EGF $NP_{21.5}$-EGF, $NP_{78.9}$-EGF + AG1478, $NP_{78.9}$-EGF + NAC, $NP_{78.9}$-EGF + trolox, $NP_{78.9}$-EGF + tempol. (b) Apoptosis enhancement for $NP_{78.9}$-EGF, $NP_{78.9}$-EGF + AG1478, $NP_{78.9}$-EGF + trolox, $NP_{78.9}$-EGF + tempol. All presented data were recorded from three independent experiments. Error bars show standard deviations. Significance was evaluated relative to the untreated control (a) or $NP_{78.9}$-EGF (b). **$p < 0.01$; *$p < 0.05$.*

When we measured the apoptosis enhancement for $NP_{78.9}$-EGF in the presence of the EGFR inhibitor or the three antioxidants (Fig. 6b), we found that the inhibition of EGFR phosphorylation through AG1478 and the reduction of oxidative stress through NAC or tempol very efficiently suppressed apoptosis. Surprisingly, the antioxidant trolox did not suppress the apoptotic efficacy of $NP_{78.9}$-EGF, instead an even higher apoptosis enhancement was detected for the combination of $NP_{78.9}$-EGF and trolox. We verified in control experiments that trolox alone did not induce apoptosis under the chosen experimental conditions (Fig. S8†), confirming that the detected gain in apoptosis enhancement resulted from a synergistic effect between $NP_{78.9}$-EGF and trolox. A potential explanation for the different effects of trolox and NAC or tempol could be related to the different chemical natures of the antioxidants. Different from the GSH precursor NAC that removes ROS by enhancing the glutathione response,[65] or the stable radical tempol whose primary reaction product after reaction with ROS is an oxoammonium cation,[66,67] trolox is converted into a reactive radical cation by reacting with ROS. The observed failure of trolox to inhibit apoptosis could, therefore, be caused by the radical nature of the reaction product. The trolox radical cation is a strong oxidant and its reactivity could result in cellular damage and other detrimental cell processes. The apoptotic effect may be further potentiated by the preferential localization of this vitamin D derivative to cellular membranes.

2.3 Discussion

The systematic analysis of NP-EGF induced apoptosis in Fig. 2 confirms that neither EGF ligand nor NP by itself results in apoptosis under the chosen experimental conditions. The observed apoptosis must, therefore, be a result of the conjugation of EGF to NP and the accompanying changes in the cellular response to the ligand and core. The EGF surface density,

NP size, and shape all interact to influence the apoptotic efficacy of nanoconjugated EGF. High EGF densities favor apoptosis, spherical NP are more effective than NR, and the largest NP investigated in this work with a diameter of 80 nm are particularly effective. NP-EGF with smaller core diameters can also induce apoptosis, but require longer co-incubation times than the 4 h applied in this work.[25] All of the investigated EGF nanoconjugates activate EGFR. Even though the effective EGF concentration was constant in all cases, the measured phosphorylation differs between the nanoconjugates (Fig. 2c). $NP_{78.9}$-EGF and NR-EGF (AR = 8.6) show higher phosphorylation levels than $NP_{21.5}$-EGF and $NP_{40.4}$-EGF. In fact, $NP_{78.9}$-EGF and NR-EGF achieve similar phosphorylation levels to 40 nM free EGF, although the effective EGF concentration of the nanoconjugates is only 1 nM. But despite the similar phosphorylation levels for free EGF (40 nM), $NP_{78.9}$-EGF, and NR-EGF, only $NP_{78.9}$-EGF effectively induced apoptosis (Fig. 2a). The observation that comparable EGFR phosphorylation levels yield different apoptosis enhancements implies that the total EGFR activation alone is insufficient to account for the observed apoptosis differences under the chosen experimental conditions. Instead, differences in the activation process that are related to the structure and ligand presentation by EGF-presenting NP seem to play a key role in the induction of apoptosis. For one, the increase in apoptosis with increasing EGF surface density in Fig. 2f confirms that multivalent EGF presentation enhances the apoptotic signaling. But the shape of the NP also plays an important role. For instance, NR-EGF (AR = 8.6) with comparable EGF surface loadings and total phosphorylation levels to $NP_{78.9}$-EGF did not induce apoptosis (Fig. 4h). We conclude that an accurate evaluation of apoptotic efficacy requires an explicit consideration of NP size, ligand density, and shape.

Based on the putative mechanism for free EGF induced apoptosis enhancement, which attributes apoptosis to the accumulation of activated EGFR in early endosomes,[12,13,15,68] it is conceivable that it is not the global EGFR signaling but specifically the endosomal EGFR signaling that is the determining factor for NP-EGF induced apoptosis enhancement. Apoptosis could then be the result of EGF nanoconjugation induced changes in the temporospatial intracellular signaling patterns of the bound EGFR. The fact that $NP_{40.4}$-EGF failed to induce comparable apoptosis levels to $NP_{78.9}$-EGF, even when the concentration of delivered EGF was much higher (Fig. 3b–d) emphasizes a central role of the physical NP size in determining the apoptotic efficacy of nanoconjugated EGF. The shape and size of a stiff NP have direct implications for the trafficking of NP-EGF tethered EGFR as vesicle sorting and trafficking require a high degree of structural flexibility, or pleomorphism, of the participating vesicles in the dense matrix of the cytoplasm.[69] Gold NP are hard, and under typical cellular conditions they are non-deformable objects. The structural flexibility of a vesicle of a given size (for instance formed through clathrin-mediated endocytosis) and, thus, its mobility in the cytoplasm are expected to decrease with the increasing size of the contained gold NP cargo.[70] Indeed, we observed higher early endosome concentrations for $NP_{78.9}$-EGF than for $NP_{21.5}$-EGF (Fig. S6†), which could result from an overall slower intracellular trafficking of the larger NP core.[26] Confocal scans also indicated some differences in the spatial distribution of EEA1 for $NP_{78.9}$-EGF, which motivate further detailed experimental investigation of the impact of NP size on the trafficking of nanoconjugated EGF.

EGFR activation is known to trigger ROS generation,[57,71] and the increase in cytoplasmic ROS and reduction of the cellular GSH/GSSG ratio observed in this work are consistent with a

persistent activation of cytoplasmic EGFR. The associated change in the cellular milieu represents a key checkpoint in EGF nanoconjugation induced apoptosis. Suppression of a drop in GSH/GSSG ratio by NAC or tempol, or inhibition of EGFR signaling through AG1478 successfully prevented NP-EGF induced apoptosis (Fig. 6). Intriguingly, the nanoconjugated EGF did not trigger increased mitochondrial ROS levels, which corroborates the hypothesis that mitochondria-independent redox signaling in the cytoplasm is the origin of EGF nanoconjugation induced apoptosis.

For ligand–receptor pairs whose signaling outcomes are spatially regulated, differences in the uptake mechanism can result in different signaling results. Importantly, for NR-EGF (AR = 8.6) we found indications of caveolae-mediated endocytosis, whereas $NP_{78.9}$-EGF was primarily taken up by clathrin-mediated endocytosis (Fig. 4j and k). A switch in the uptake mechanism from clathrin- to caveolae-mediated endocytosis for nanorods with a length of around 80 nm is in good agreement with the previous findings by Liu *et al.*[42] A transition from clathrin- to caveolae-mediated uptake changes the temporospatial distribution of the nanoconjugated EGF (and the bound EGFR). In addition, caveolin-1, which is a component of caveolae, can downregulate the EGFR signaling by dephosphorylating the receptor tyrosine kinase.[72–74] We, consequently, attribute the observed differences in the apoptotic efficacy of high AR NR and larger NP to a reduction of oxidative stress due to shape-dependent differences in the uptake and intracellular signaling of EGFR. Additional studies into the cellular mechanisms underlying the shape-dependent differences in oxidative stress upon the uptake of nanoconjugated EGF are warranted.

2.4 Conclusion

NP–cell interactions are complex and can result in unexpected and potentially harmful signaling outcomes for nanoconjugated ligands targeted at cell surface receptors. If these interactions are understood in detail, they provide, however, also new opportunities for manipulating and controlling cell signaling. In this work, we have demonstrated that nanoconjugation modulates the apoptotic efficacy of EGF and that the magnitude of the effect depends not only on the ligand density of the NP but, in particular, on the size and shape of the NP core. Under the chosen experimental conditions, $NP_{78.9}$-EGF was much more efficient in inducing apoptosis than smaller NP or high AR NR with comparable EGF loading. Apoptosis was shown to be related to $NP_{78.9}$-EGF induced oxidative stress. Cytoplasmic ROS generation and perturbation of the glutathione homeostasis were key events for EGF nanoconjugation mediated apoptosis and their abrogation prevented apoptosis. The successful induction of apoptosis in cancer cells through nanoconjugated EGF is particularly important and has translational potential as apoptosis evasion is one of the hallmarks of cancer and the established EGFR targeted therapeutics suffer from rapid development of resistance.[75]

3 Chapter 3

Epidermal Growth Factor Presenting Polymer Nanoparticles Stimulate Nitric Oxide Generation and Modulate Apoptotic Signaling through Nitrosylation of JNK

3.1 Introduction

Epidermal growth factor (EGF) is usually associated with cell growth and proliferation but it has long been known that under certain conditions EGF binding to its receptor (EGFR) can also induce apoptosis.[1-3] Intriguingly, it was found that conjugation of EGF to a nanoparticle (NP) enhances EGF-induced apoptosis, as indicated by increased caspase-3 activity, nucleus condensation, phosphatidylserine translocation and changes in cell morphology.[4-6] The data available so far suggest that the NP-EGF-induced apoptosis arises from a perturbation of the spatial regulation of EGFR signaling due to an accumulation of activated EGFR in early endosomes. This behavior is consistent with studies on "free" EGF that have shown that accumulation of activated EGFR in early endosomes is a key factor for apoptosis induced by EGF.[7-10] The intracellular mechanisms that couple spatial dysregulation of activated EGFR upon NP-EGF binding to apoptosis remain, however, incompletely understood. Initial studies on nanoconjugated EGF have shown that increased levels of reactive oxygen species (ROS) are an important factor in NP-EGF-mediated apoptosis.[6] The observation of an increase in ROS after NP-EGF binding and uptake raises important questions as to whether reactive nitrogen species (RNS), in particular nitric oxide (NO), are also increased after NP-EGF binding and what role NP-EGF-induced NO plays in the induction of apoptosis. Characterizing the role of the small, lipophilic molecule NO in NP-EGF-induced apoptosis is of great interest as NO has important biological regulatory functions with direct relevance to apoptosis.

NO is a reactive and volatile small molecule that is regulated by control of its synthesis through nitric oxide synthases (NOS). Importantly, previous studies have revealed that

EGF can activate inducible NOS and trigger increased NO levels.[11-13] If present in small quantities, NO represents a signaling molecule that functions as a second messenger.[14] Regulatory functions of NO derive from the molecule's general redox-reactivity, for instance, in the nitrosylation of thiols in kinases and caspases and other enzymes, as well as from its specific recognition through NO receptors.[15-19] The diffusion length and, thus, the radius of activity of an individual NO molecule is limited through its reactivity and the associated "reactive quenching". In fact, if NO is present at high concentrations, off-target NO-driven redox reactions can cause significant cellular damage. The role of NO in cancer is complex[20] and the molecule has been observed – depending on its concentration – either to promote proliferation, enhance invasiveness and metastasis, and repress apoptosis or to induce oxidative stress and trigger apoptosis.[21-24] Interestingly, NO is particularly relevant for the disease progression in the BLBC subtype which primarily display a triple negative (ER-, PR- and HER2-) phenotype accounting for 15% of all breast cancers.[17,25-32] BLBC has poor prognosis and remains difficult to treat [33,34] and, therefore, there is an urgent need for development of new robust cancer inactivation strategies. Since some BLBCs express EGFR,[35] NP-EGF-induced apoptosis could pave the path to a potential strategy to target this subset of cancers, provided the mechanisms of NP-EGF-induced apoptosis and the interplay of ROS and NO are understood in greater detail.

In the current study, we investigate how the nanoconjugation of EGF affects intracellular NO levels in an EGFR-overexpressing BLBC cell model (MDA-MB-468), in BLBC cells with medium EGFR expression levels (MDA-MB-231), and in $Her2^{+}$ control cells (SKBR3) with low EGFR expression levels and establish a correlation between NO levels

and NP-EGF-induced apoptosis, as measured by caspase-3 activity.[36] As NO has been reported to have both pro-apoptotic as well as cell-protective functions, we monitored the effect of NP-EGF on apoptosis both in the presence and absence of NO scavenger.

3.2 Methods

3.2.1 *PLGA-lipid-EGF NP (NP-EGF) synthesis and functionalization.*

The NP preparation followed the method described by Mandal *et al*[37] ***optimized by Behnaz Eshaghi.*** 2.5 mg of PLGA powder (lactide:glycolide 50:50, M_w = 24,000-38,000) was dissolved in 1 mL of anhydrous acetonitrile to prepare the polymer solution. 8 µL of 25 mg/mL 1,2-distearoyl-sn-glycero-3-phosphoethanolamine-N-[azido(polyethylene glycol)-2000] (ammonium salt) (DSPE-PEG(2000)-azide) and 5 µL of 16:0 1,2-dipalmitoyl-sn-glycero-3-phosphoethanolamine-N-(lissamine rhodamine B sulfonyl) (ammonium salt) (Liss Rhod PE) were added to 4 mL of MilliQ water (18 MΩ×cm). 400 µL of PLGA solution was added dropwise to the lipid-water mixture and the mixture was sonicated for 5 min at room temperature followed by a brief vortexing to homogenize the synthesized PLGA-lipid NP dispersion. The NP dispersion was then washed twice by centrifugation using 4mL 10K Nominal Molecular Weight Limit (NMWL) Amicon® Ultra-4 Centrifugal Filters. 2 µL of a 100 mg/mL propargyl-N-hydroxysuccinimidylester ($C_{10}H_{11}NO_5$) solution in DMSO was added to 100 µL of 1mg/mL EGF and incubated on ice for 6 h. The mixture was dialyzed against 1x PBS for 72 h. 150 µL PLGA-lipid NP dispersion was then incubated overnight with 25 µL of the prepared functionalized EGF at 4°C in 500 µM ascorbic acid and 100 µM CuSO4 (catalyst for the cycloaddition reaction) containing buffer. The resulting NP-EGF was then washed twice by centrifugal filters prior to resuspension in DMEM.

3.2.2 *NP surface EGF quantification.*

The amount of NP-loaded EGF was quantified using a EGF Human ELISA Kit (Invitrogen). Briefly, NPs were diluted to reach a concentration of 2 pM and then incubated in an antibody-coated 96-well plate provided in the kit. Total EGF concentrations in the samples were determined following the protocol provided by the vendor. The number of EGF per NP were then calculated. The EGF concentration in the supernatant of the NP samples after the last wash was also quantified to detect any possible undesired free EGF in the NP samples.

3.2.3 Caspase-3 activity measurements.

MDA-MB-468, MDA-MB-231, and SKBR3 cells were cultured in 6-well plates in DMEM-10% FBS at a density of $1*10^5$/mL. After 80% confluency was reached, the cell medium was removed and replaced with fresh DMEM containing NP samples or controls. The plate was incubated for 4 h at 37°C in the presence of 5% CO_2. Cells were then washed 3x with Hank's buffer and incubated for additional 20 h in DMEM-10% FBS at 37°C in the presence of CO_2. Cells were collected by trypsinization and washed with 1x PBS by centrifugation. EnzChek® Caspase-3 Assay Kit was used to quantify caspase-3 activity in the samples. Total protein concentration in samples were also quantified using Pierce BCA Protein Assay Kit to account for the differences in the sample size. Apoptosis enhancement relative to the control cell samples with no treatment were calculated based on the caspase-3 activity levels.

3.2.4 Quantification of NP cellular uptake.

After 4 h of incubation of NPs with cells in DMEM (NP concentration: 100 pM), cells were washed with 1x PBS and the cell density was quantified using a hemacytometer. After lysing of the cells, the sample fluorescence was quantified in a 96-well plate using a SpectraMax M5 plate reader. Known concentrations of NPs were used as the standard curve to calculate NP concentration in the lysate. The number of NPs per cell was then calculated based on the total number of NPs and total number of cells in the sample.

3.2.5 ROS quantification.

Cytoplasmic ROS was quantified using a CellROX Deep Red Flow Cytometry Assay Kit (Invitrogen). Briefly, cells were incubated with desired samples with DMEM for 4 hrs. Following cells incubation with fluorogenic CellROX™ Deep Red Reagent, cells were trypsinized and washed with 1X PBS and analyzed with flow cytometry for fluorescence quantification.

3.2.6 Nitric Oxide quantification.

Cellular NO levels were quantified using a Nitric Oxide Assay Kit (Invitrogen™). After 4 h of incubation, the cells were detached, washed with 1x PBS, and lysed before NO quantification.

3.2.7 Western Blot.

Cells were incubated with desired samples and controls for 4 h, detached, washed with 1x PBS, and lysed with cell extraction buffer (Invitrogen™). Total protein concentrations were quantified using Bio-Rad Protein Assay Dye Reagent Concentrate. All samples were diluted to the concentration of the sample with the lowest concentration before gel electrophoresis. Samples were mixed with NuPAGE lithium dodecyl sulfate (LDS) sample buffer and NuPAGE sample reducing agent and then incubated at 70°C for 10 min. Samples were loaded in NuPAGE 4-12% Bis-Tris gels and run at 100 V for 2 h at room temperature followed by transfer to a membrane at 4°C for overnight. Membranes were blocked in tris-buffered saline and polysorbate 20 (TBST)-5% non-fat dry milk (NFDM) for 30 min followed by primary antibody incubation overnight at 4°C. The membrane was washed 3x with TBST and incubated with peroxidase-conjugated secondary antibody for 30 min. Membrane was washed 3x with TBST and incubated for 30 s in chemiluminescent substrate, and was finally imaged using a BioRAD ChemiDoc™ XRS+ System.

3.2.8 Detection of protein S-Nitrosylation.

Cells were incubated with desired samples and controls for 4 h, detached, and washed with 1x PBS. Protein S-Nitrosylation was detected using Pierce™ S-Nitrosylation Western Blot Kit. Briefly, samples were lysed by HENS buffer (100 mM HEPES (pH 7.8), 1 mM EDTA, 0.1 mM neocuproine, and 1% SDS) provided in the kit, labeled by iodoacetyl tandem mass tag (iodoTMT) Reagent, and detected by anti-TMT antibody through Western Blotting.

3.2.9 Inhibitors and Scavengers.

AG1478, an EGFR-specific RTK inhibitor,[38] was used at a concentration of 500 nM. AG1478 was initially dissolved in DMSO and then diluted to the final concentration in DMEM. SP600125 JNK inhibitor[39] was used at a concentration of 25 μM. Carboxy-PTIO,[40] a selective NO scavenger, was used at a concentration of 1 mM during the initial 4 h of NP treatment and then at a concentration of 100 μM for the subsequent 20 h incubation after NP removal.

3.3 Results and Discussion

NP-EGF with Polymer Core Trigger Apoptosis in EGFR-overexpressing BLBC Cell Line. We used the lipid-wrapped poly(lactic-co-glycolic acid), PLGA, NPs schematically outlined in **Figure 1a** as platform to create NP-EGF of defined size and surface loading. The biodegradable PLGA core represents a scaffold with defined size, and the biomimetic membrane layer provides control over the surface properties of the NPs and facilitates the integration of azide-modified lipids to covalently tether alkyne-modified EGF through the Cu(I)-catalyzed 1,3-dipolar cycloaddition[41]. The lipid layer was composed of fluorescent 16:0 1,2-dipalmitoyl-sn-glycero-3-phosphoethanolamine-N-(lissamine rhodamine B sulfonyl) (ammonium salt), referred to in the following as Liss Rhod PE, and 1,2-distearoyl-sn-glycero-3-phosphoethanolamine-N-[azido(polyethylene glycol)-2000] (ammonium salt), in the following referred to as DSPE-PEG2000-N_3, in the ratio 5:95. **Figure 1b** shows the hydrodynamic diameter determined by dynamic light scattering (DLS) for PLGA NP preparations before and after wrapping the core in a lipid-PEG layer; an increase in average diameter from 80 ± 4 nm to 88 ± 4 nm is observed. The zeta potential of the NPs was -28.5 mV and -22.5 mV before and after membrane wrapping. Binding of EGF to the NPs further increased the hydrodynamic diameter to approx. 100 nm. The number of EGF peptides bound per NP was determined by ELISA to be 64 ± 6 (**Figure 1c**). The supernatant did not show any residual EGF, ensuring that all cellular effects are exclusively caused by nanoconjugated EGF. Unless otherwise noted we used NP-EGF with a hydrodynamic diameter of approx. 90 nm and effective EGF concentration of approx. 6 nM throughout this work.

Since previous studies demonstrating enhanced, EGF-induced apoptosis upon nanoconjugation were all performed with gold NPs[4-6], we first verified that the softer, biodegradable polymer NPs also induce apoptosis. We tested the apoptotic effect of the EGF-loaded NPs (NP-EGF) *in vitro* with the EGFR overexpressing BLBC *in vitro* cell model, MDA-MB-468. NP-EGF binding and uptake in these cells was EGF-specific

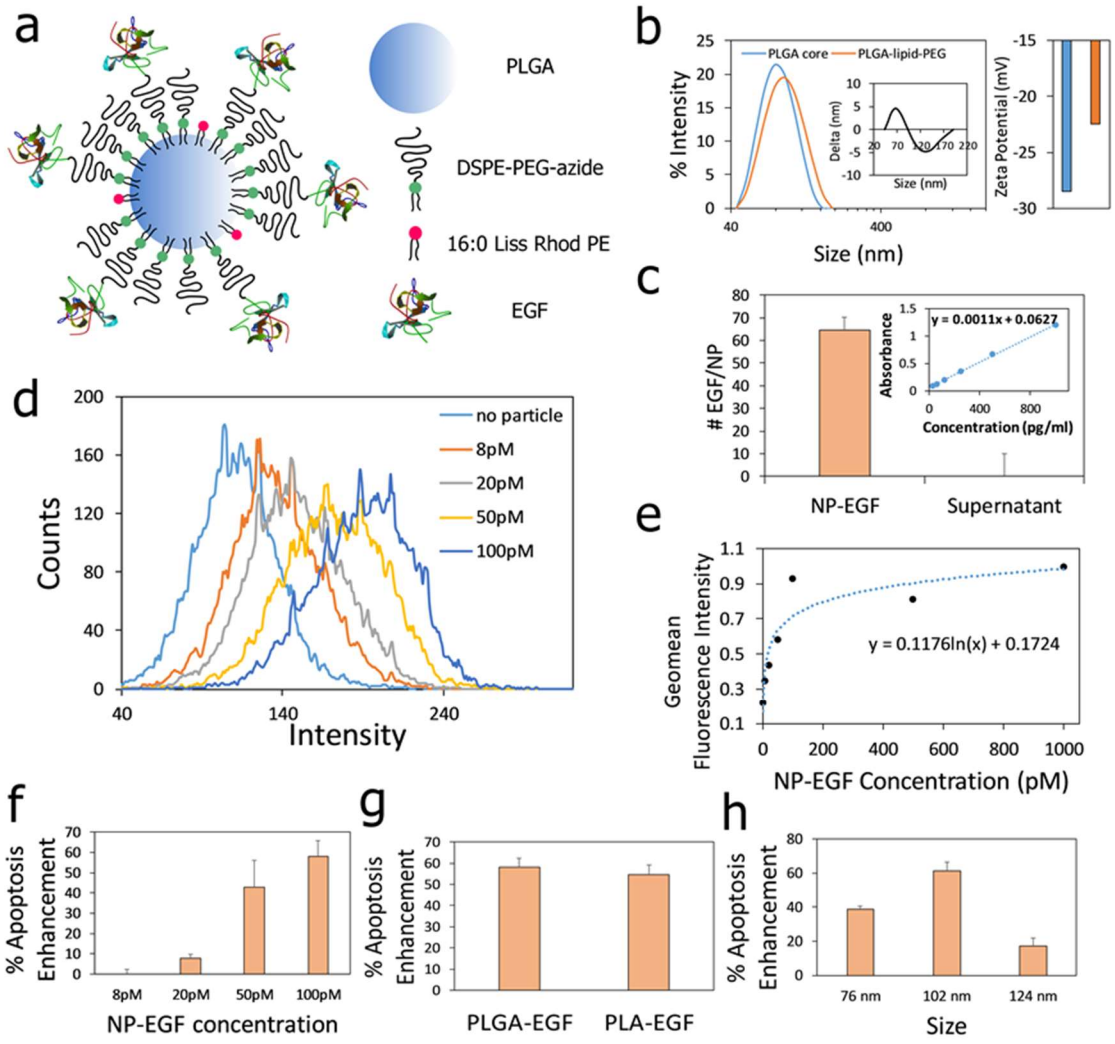

Fig. 3-1 a) Scheme of NP EGF-functionalized NPs (NP-EGF). b) Hydrodynamic diameter distribution (left) and zeta potential (right) of PLGA NPs before and after wrapping with lipid-PEG layer. Inset shows the calculated difference between NP size distributions recorded after and before wrapping with lipid-PEG layer. c) Number of EGF per NP quantified by ELISA. d,e) Uptake of NP-EGF after 4 hours incubation in DMEM as function of input concentration determined by FACS. f) Apoptosis enhancement of PLGA-EGF after 24 h (4h NP incubation + 20 h post-incubation after excess NP removal) as a function of NP input. g) Apoptosis enhancement induced by 100 pM PLGA-EGF and PLA-EGF (4h NP incubation + 20 h post-incubation after excess NP removal). h) Apoptosis enhancement induced by different sizes of PLGA-EGF (100 pM).

(**Figure 1d**) and concentration dependent (**Figure 1e**). After an initial steep increase of uptake as function of concentration, the increase in uptake levels off for concentrations ≥ 100 pM, indicative of a saturation of uptake.

To quantify the apoptotic effect of the NPs, we incubated MDA-MB-468 cells with NP-EGF concentrations of 8 pM, 20 pM, 50 pM, 100 pM for 4h. The NP solution was then removed and the cells were maintained in cell medium at 37˚C for another 20 h before caspase-3 levels were quantified and apoptosis enhancements in % relative to the no treatment control were calculated. Consistent with the trends for NP-EGF uptake we detected an increase in apoptosis with increasing NP-EGF input (**Figure 1f**). For a NP-

EGF input concentration of 100 pM (effective EGF concentration 6 nM), we reliably measured an average apoptosis enhancement (relative to the no treatment control) of approximately 58% in EGFR overexpressing MDA-MB-468. We did not detect increased apoptosis levels for NP-EGF in the BLBC cell line with low EGFR expression level (MDA-MB-231) or luminal cells (SKBR3) under the same experimental conditions (*vide infra*). However, the strongly EGFR over-expressing epidermoid carcinoma cell line A431 also showed greatly increased levels of apoptosis (**Figure S1**), suggesting that the apoptosis-enhancing effect is common in other EGFR-overexpressing cancer cells. In a second set of experiments we replaced PLGA with polylactic acid (PLA) as core material and observed similar levels of apoptosis enhancement in MDA-MB-468 (**Figure 1g**), confirming that the apoptotic effect is largely independent of the choice of the polymer core material.

The maximum apoptosis enhancement for the polymeric NPs investigated in this work are comparable with the maximum apoptosis enhancements observed previously for EGF-presenting 80 nm gold NPs.[4-6] It must be emphasized, however, that the gold NPs achieved this effect at a much lower input concentration. An 8 pM solution of gold NP-EGF was sufficient to yield the same maximum phosphorylation as a 100 pM solution of polymeric (PLGA, PLA) NP-EGF. In contrast, an 8 pM solution of polymeric NP-EGF did not show any significant increase in apoptosis. The polymer NPs used in this work had glass transition temperatures lower than 37°C and were, thus, quite soft. The difference in apoptotic efficacy between metal and polymer core NP-EGF may be related to differences

in the core stiffness (polymer vs. metal), which can change the intracellular trafficking[42-47] and, thus, affect the spatial regulation of EGFR signaling. Alternatively, the effect could also be due to differences in the uptake of NPs with different densities (gold *versus* polymer) in the cell-culture based approaches. A further analysis of the NP core specific differences is ongoing but goes beyond the scope of this work. The key finding of this section is that EGF-presenting polymer NPs can induce apoptosis in EGFR overexpressing

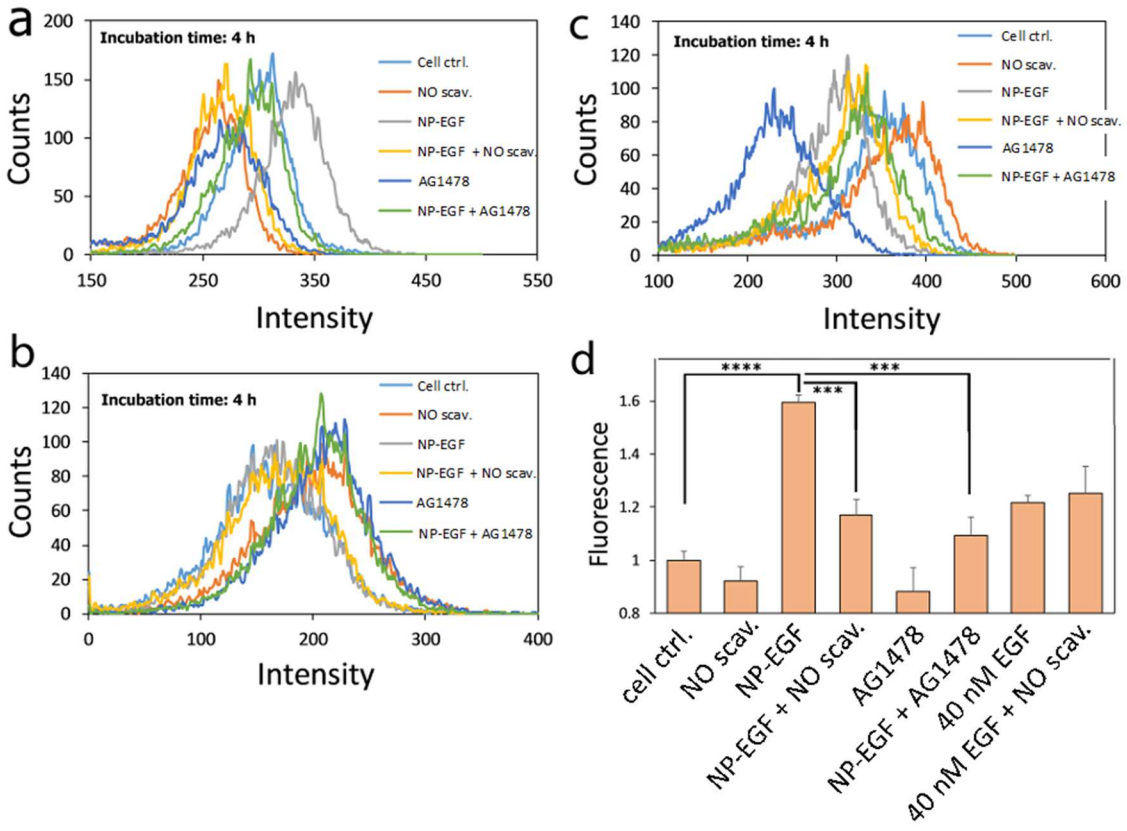

Fig. 3-2 a) Cellular ROS levels of MDA-MB-468 cells measured using the CellRox indicator by FACS. The effect of EGF-functionalized PLGA NP (90 nm diameter, 100 pM input concentrations) with and without NO scavenger (Carboxy-PTIO) (1 mM) and EGFR-

specific RTK inhibitor AG1478 (500 nM) was quantified. A no-treatment control was included as reference. b) Cellular ROS levels of MDA-MB-231 cells and c) SKBR3 cells after 4 h of incubation. d) Intracellular NO levels as determined by nitric oxide assay (Invitrogen™) for MDA-MB-468. Data are averages over two independent repeats.

BLBC cells. Even if polymer NPs require higher concentrations than metallic NPs, they offer the advantages of biodegradability and higher general biocompatibility.

We evaluated the dependence of the apoptotic effect on the size of the NP samples by measuring the apoptosis obtained with PLGA NP-EGF with average hydrodynamic diameters of 76 ± 4 nm, 102 ± 5 nm, and 124 ± 6 nm at a constant NP input concentration of 100 pM (**Figure 1h**). We found that the NPs with intermediate size provided the strongest enhancement of apoptosis.

3.3.1 NP-EGF-Induced Reactive Oxygen Species (ROS) and NO Formation.

Induced oxidative stress is an important factor in NP-associated toxicity,[48-50] and it is also known to play a role in the apoptosis observed for NP-EGF with gold core.[6] We measured the general cellular oxidative stress (defined by hydroxyl radicals, superoxides, peroxynitrites, NO) in response to PLGA NP-EGF (100 pM) and for the same NPs in the presence of the EGFR-specific kinase inhibitor AG1478[38], or NO scavenger Carboxy-PTIO[51] using a fluorescence (CellRox) indicator for MDA-MB-468 (**Figure 2a**), MDA-MB-231 (**Figure 2b**), and SKBR3 (**Figure 2c**) cells. No-treatment controls and controls with AG1478 or Carboxy-PTIO in the absence of NP-EGF were included in all our measurements.

For MDA-MB-468 (**Figure 2a**) we found that NP-EGF addition induces significant levels of oxidative stress but that both AG1478 and the NO-specific scavenger Carboxy-PTIO reduce this stress. Interestingly, while AG1478 lowers the oxidative stress to the cellular background of the no-treatment controls, the NO scavenger reduced the oxidative stress even below the levels of the no-treatment control. Together, these findings imply i.) that NP-EGF-induced oxidative stress in MDA-MB-468 is EGFR-dependent, ii.) that NO contributes significantly to the measured oxidative stress, and iii.) that the intracellular NO levels are already non-negligible even in the absence of any NP challenge. In MDA-MB-231 (**Figure 2b**) AG1478 inhibitor and NO scavenger both trigger an increase in oxidative stress, but the total oxidative stress observed for NP-EGF is essentially identical to the no treatment control. In SKBR3 (**Figure 2c**), NP-EGF addition even reduces the oxidative stress relative to the no treatment control. NO scavenger and AG1478 (in the presence of

the NP-EGF) increase oxidative stress, while AG1478 alone achieves a strong reduction. In conclusion, for the chosen NP-EGF concentrations (100 pM) and exposure times (4 h) only the EGFR overexpressing BLBC model MDA-MB-468 exhibits a NP-EGF-induced increase in ROS levels that is reversed by NO scavenger. The striking differences in the effect of AG1478 and NO scavenger on the oxidative stress in the different cell lines underlines the complex, cell-specific regulation of ROS and NO generation.

To further characterize the contribution of NO to the detected oxidative stress in MDA-MB-468, we measured the intracellular NO levels with a dedicated NO assay (**Figure 2d**). This essay confirmed significantly increased levels of NO after addition of NP-EGF. NO scavenger and AG1478 both successfully inhibited an increase in intracellular NO in response to NP-EGF. These finding provide experimental evidence that the increase in intracellular NO is related to the activation of EGFR. We also measured the NO levels obtained for a 40 nM solution of free EGF, corresponding to a > 6-fold higher effective EGF concentration than in the case of NP-EGF. Despite the higher EGF concentration, the measured NO levels were lower for free EGF. We conclude that NP-EGF is particularly effective in inducing apoptosis.

3.3.2 ***Effect of NO Scavenger on NP-EGF-Induced Apoptosis.*** The published literature suggests that the effect of NO on cancer cells is concentration-dependent.[16,52] While low concentrations < 100 nM generally favor proliferation and metastasis, higher concentrations > 400 nM can cause cytotoxicity and apoptosis.[20,53,54] In the absence of NO scavenger we observed an apoptosis enhancement of up to ~58% in MDA-MB-468 but noted no increase in MDA-MB-231 or SKBR3 (**Figure 3**). We quantified the effect of the NO-specific scavenger Carboxy-PTIO for all three investigated cell lines. The concentration of the scavenger added was 1 mM for the first 4 h and 100 μM for the subsequent 20 h. The NO scavenger treatment by itself led to apoptosis enhancements of approximately 60% (MDA-MB-468), 50% (MDA-MB-231), 20% (SKBR3) (**Figure 3**). The apoptosis-enhancing effect of the NO scavenger implies that the NO concentrations in these cells lie in a range that is associated with a pro-survival (anti-apoptotic) role. After characterizing the separate effects of NP-EGF and NO scavenger, we next evaluated the synergistic effects that arise through combination of NP-EGF and Carboxy-PTIO. To that end, we co-incubated NP-EGF (100 pM) and NO scavenger (1 mM) with the cells for 4 h and subsequently maintained the cells after removal of the NPs for another 20 h

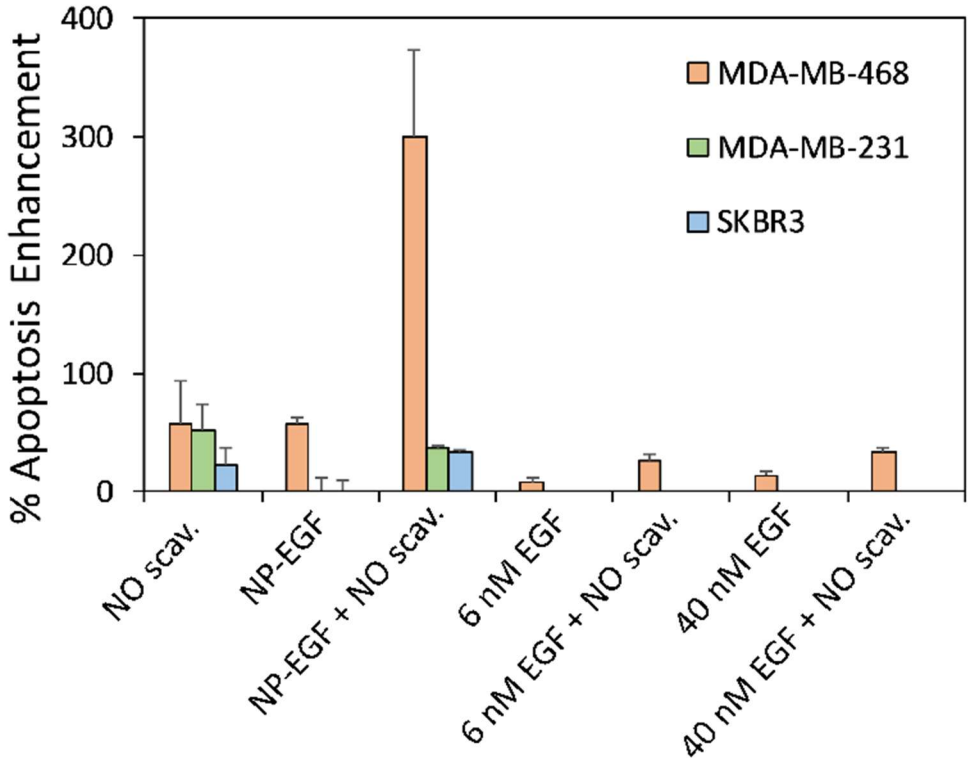

Fig. 3-3 Apoptosis enhancement measured for basal, EGFR-overexpressing MDA-MB-468, basal MDA-MB-231 with low EGFR expression, and luminal, EGFR-overexpressing SKBR3 for (from left to right): NO scavenger, NP-EGF (100 pM), NP-EGF + NO scavenger, 6 nM EGF, 6nM EGF + NO scavenger, 40 nM EGF, 40 nM EGF + NO scavenger. All experiments were performed as duplicates and repeated for six times.

3.3.3 in the presence of NO scavenger at a concentration of 100 µM. Intriguingly, addition of NP-EGF in the presence of NO scavenger dramatically increased apoptosis in MDA-MB-468 cells. We measured an average apoptosis enhancement of 300±73%. This strong increase was unique for the EGFR-overexpressing BLBC cell line MDA-MB-468. Neither the SKBR3 nor MDA-MB-231 cells showed a similar behavior; both had constant or even slightly declining apoptosis enhancements when treated with NO scavenger. Control experiments obtained with 6 nM and 40 nM solutions of free EGF under otherwise identical conditions showed no detectable apoptosis enhancement for SKBR3 or MDA-MB-231 and only low enhancement for MDA-MB-468, confirming that the apoptosis enhancing effect in the presence of NO scavenger was unique to nanoconjugated EGF.

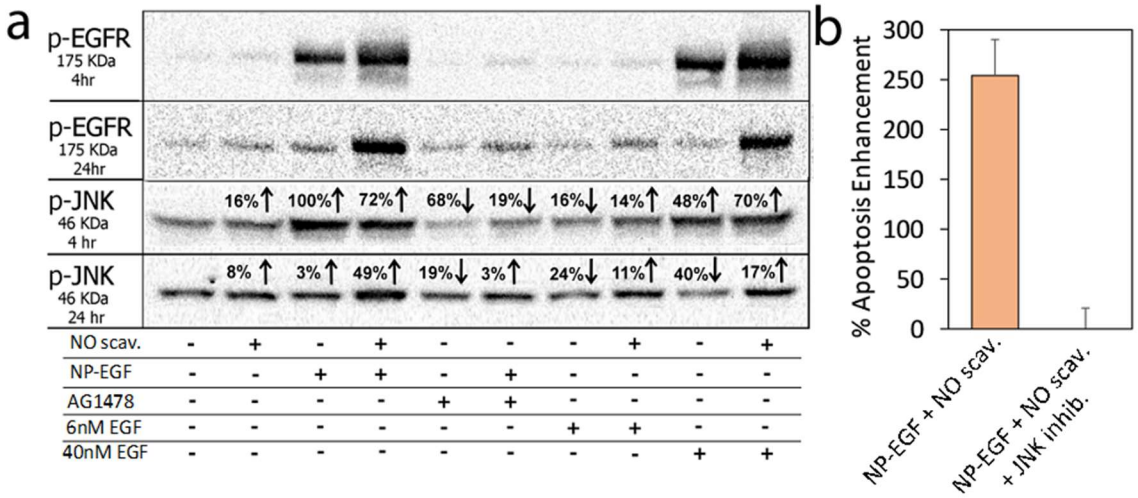

Fig. 3-4 Characterization of EGFR and JNK phosphorylation through Western Blots. a) From top to bottom: phosphorylation of EGFR after 4h; phosphorylation of EGFR after 24 h; phosphorylation of JNK after 4 h; phosphorylation of JNK after 24 h. NP-EGF concentration is 100pM. NO scavenger concentration is 1mM for the first 4 h and 100 µM

for the next 20 h incubation. AG1478 and JNK inhibitor concentrations are 500nM and 25 μM, respectively for the entire 24 h of incubation. For pJNK the relative increase (↑) or decrease (↓) in intensity in % relative to the no treatment control are added for each band. b) Apoptosis enhancement of NP-EGF + NO scavenger and NP-EGF + NO scavenger + JNK inhibitor.

3.3.4 Effect of NO on MAPK Activation in EGFR-overexpressing MDA-MB-468.

Mitogen-activated protein kinases (MAPK) control important regulatory functions in cell growth, development and apoptosis and orchestrate cellular responses to external stress. It is known that MAPKs contribute to the control of cellular NO levels and that NO can activate several MAPK pathways.[55-59] It is, thus, conceivable that MAPKs also play a role in facilitating the synergistic enhancement of apoptosis in the presence of both NP-EGF and Carboxy-PTIO. To test this hypothesis, we analyzed the impact of NP-EGF +/- Carboxy-PTIO on the activation (measured as phosphorylation) of the three main MAPK sub-families: extracellular signal-regulated protein kinase (ERK), p38, and c-Jun-terminal kinases (JNK). We did not detect any NP-EGF-induced changes in either ERK or p38 activation levels (**Figure S2**), but for JNK, NP-EGF addition resulted in a measurable increase in phosphorylation. This is demonstrated in **Figure 4a** with Western Blots of phosphorylated EGFR and JNK under the specified conditions for two time points: 4 h and 24 h. Free EGF with concentrations of 6 nM and 40 nM were added as controls. The Western Blots show that NP-EGF (effective EGF concentration of 6 nM) and 40 nM free EGF induce a strong increase in EGFR phosphorylation after 4 h. After 24 h the EGFR phosphorylation remains strong for NP-EGF and 40 nM free EGF only in the presence of NO scavenger. Thus, one effect of the NO scavenger is to induce increased levels of phosphorylated EGFR for prolonged times.

Both NP-EGF and 40 nM free EGF also induce a measurable increase in phosphorylation of JNK at the 4 h time point in the presence or absence of NO scavenger. After 24 h the

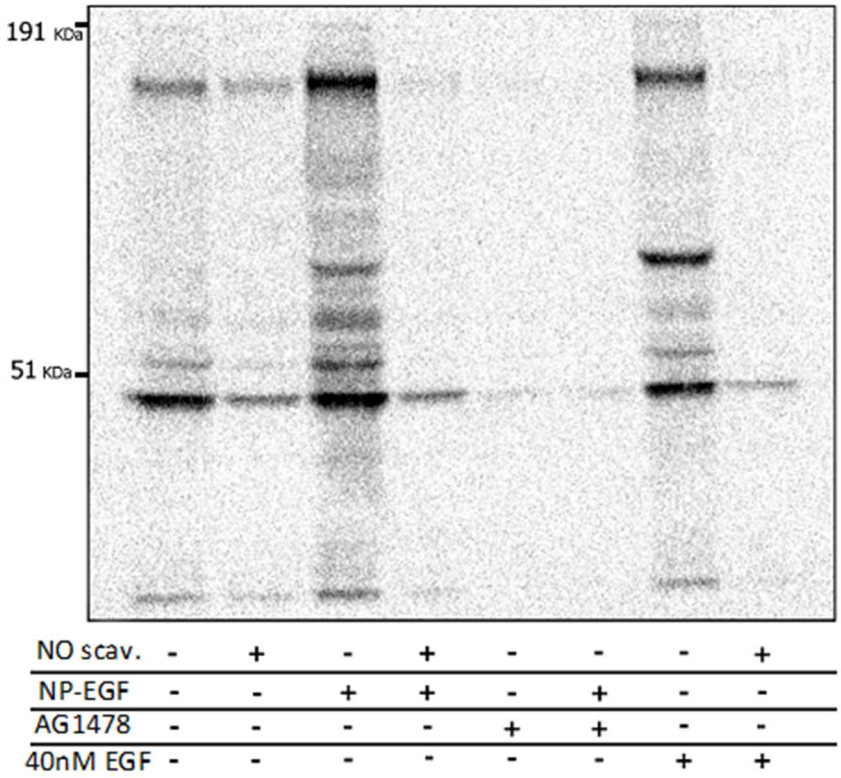

Fig. 3-5 Western Blot analysis of S-nitrosylation of the lysate of NP-EGF treated cells (4 h) for the conditions specified.

JNK phosphorylation has overall decreased, but the phosphorylation for NP-EGF in the presence of NO scavenger remains higher than for all other experimental conditions. The phosphorylation in this case is 49% higher than for the no treatment control and 32% higher than for 40 nM free EGF with NO scavenger. We also evaluated the impact of NP-EGF and NO scavenger on the total JNK concentration, which is included in **Figure S3**. We did not detect any significant difference in total JNK concentration relative to the cell control for the investigated conditions.

Considering the pro-apoptotic function of JNK,[60,61] the observation of increased levels of JNK activation over prolonged time as response to NP-EGF in the presence of NO scavenger provides a natural explanation for the observed apoptosis under these conditions. To further validate the model of a JNK-mediated apoptosis that is attenuated by NO, we measured the apoptosis for NP-EGF + NO scavenger in the absence and presence of JNK inhibitor (**Figure 4b**). Indeed, addition of JNK inhibitor effectively suppressed the observed apoptosis levels in response to NP-EGF.

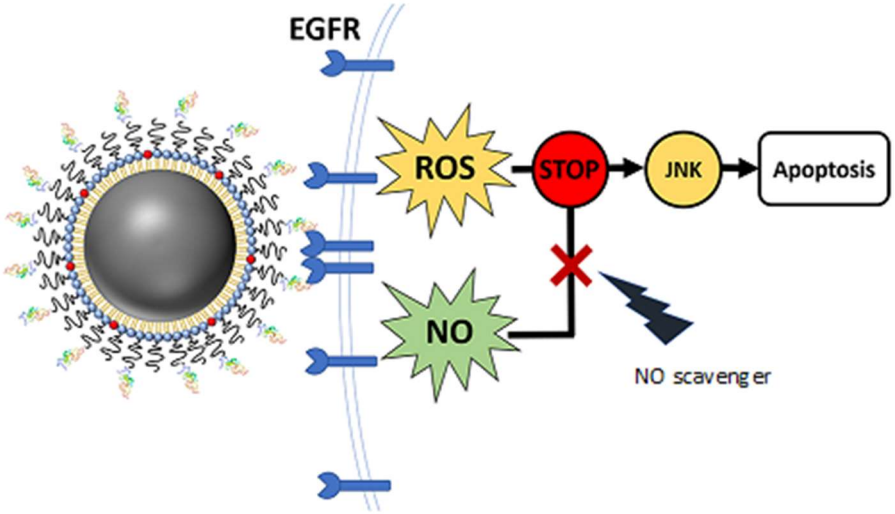

Fig. 3-6 Regulation model of NP-EGF-induced apoptosis. NP-EGF binding to EGFR triggers increased intracellular levels of NO and ROS. In the absence of NO scavenger NO nitrosylates JNK and blocks ROS-mediated activation. In the presence of NO scavenger, JNK can be phosphorylated and induces apoptosis.

3.3.5 *Nitrosylation of JNK and its Role in Regulating NP-EGF-Induced Apoptosis.*

Why does addition of NO inhibitor increase JNK phosphorylation and, thus, enhance apoptotic signaling in response to NP-EGF? It is well known that NO can nitrosylate thiols and that this oxidation can have regulatory functions. In fact, nitric oxide was shown in a different context to negatively regulate JNK (46 kDa) activity through S-nitrosylation.[62] To validate the regulatory role of JNK nitrosylation in NP-EGF-induced apoptosis, we characterized protein nitrosylation through Western Blotting. **Figure 5** shows the nitrosylation for the following conditions (left to right): cell control, carboxy-PTIO, NP-EGF, NP-EGF + carboxy-PTIO, AG1478, NP-EGF + Ag1478, 40 nM EGF+carboxy-PTIO. Both NP-EGF as well as 40 nM free EGF increase the overall nitrosylation but the effect is approximately 50% stronger for NP-EGF. Importantly, addition of NO scavenger effectively blocked nitrosylation in both cases. Given the strong NP-EGF-induced nitrosylation and the effect of NO inhibitor, we suggest the regulation model shown in **Figure 6** to account for the synergistic interplay between NP-EGF and NO inhibitor in enhancing apoptosis in MDA-MB-468. NP-EGF binding to EGFR in the plasma membrane of MDA-MB-468 results in increased intracellular levels of ROS and NO. The induced increased NO levels promote nitrosylation of JNK. Although high intracellular ROS levels in principle trigger apoptosis *via* JNK,[60,63] this signaling pathway is blocked due to JNK nitrosylation. If, however, nitrosylation is mitigated through addition of NO inhibitor, JNK phosphorylation is accessible and apoptosis related signaling is activated. Intriguingly, according to

this model one NP-EGF-induced reactive species (NO) down-regulates the apoptotic effect of the other reactive species (ROS), resulting in an effective attenuation of apoptosis signal in the cancer cell.

3.4 Conclusion

We have shown that EGF-presenting, lipid-wrapped PLGA NPs (NP-EGF) induce EGFR-dependent apoptosis in the EGFR-overexpressing BLBC cell line MDA-MB-468. Under identical experimental conditions, NP-EGF did not induce apoptosis in BLBC cells with lower EGFR expression levels (MDA-MB-231) or $Her2^+$ SKBR3 cells. For MDA-MB-468, EGFR activation through NP-EGF triggered a strong increase in intracellular ROS and NO levels. The increase in NO was associated with a nitrosylation of JNK, which effectively blocked JNK activation. In the presence of NO inhibitor, this JNK inhibition was removed and JNK-mediated apoptosis occurred. BLBC is an aggressive cancer with poor prognosis and limited options for therapy,[33,34] as BLBC cells have characteristically low expression levels of steroid hormone receptors and human epidermal growth factor 2 (Her2), a subset of BLBCs overexpress, however, EGFR which makes them potential targets for NP-EGF.[35] The synergistic interplay of NP-EGF with biodegradable polymer core and NO inhibitor to induce apoptosis selectively in EGFR overexpressing cells, demonstrated in this study, paves a new path towards inactivating at least a subset of BLBCs with targeted therapy.

4 References

4.1 Chapter 1

[1] B. K. Lee, Y. H. Yun, and K. Park, "Smart nanoparticles for drug delivery: Boundaries and opportunities," *Chemical Engineering Science*, vol. 125, pp. 158–164, 2015.

[2] Reprinted from publication title vol. 16, no. 7–8, pp. 262–271, 2013. F. J. Heiligtag and M. Niederberger, "The fascinating world of nanoparticle research," *Materials Today*, copyright (2013) with permission from Elsevier

[3] W. Fritzsche and T. A. Taton, "Metal nanoparticles as labels for heterogeneous, chip-based DNA detection," *Nanotechnology*, vol. 14, no. 12, 2003.

[4] H. Li and D. Xu, "Silver nanoparticles as labels for applications in bioassays," *TrAC - Trends in Analytical Chemistry*, vol. 61, pp. 67–73, 2014.

[5] A. Bhirde, J. Xie, M. Swierczewska, and X. Chen, "Nanoparticles for cell labeling," *Nanoscale*, vol. 3, no. 1, pp. 142–153, 2011.

[6] A. M. Schrand, L. K. Braydich-Stolle, J. J. Schlager, L. Dai, and S. M. Hussain, "Can silver nanoparticles be useful as potential biological labels?," *Nanotechnology*, vol. 19, no. 23, 2008.

[7] X. Yu, J. Wang, A. Feizpour, and B. M. Reinhard, "Illuminating the lateral organization of cell-surface CD24 and CD44 through plasmon coupling between Au nanoparticle immunolabels," *Analytical Chemistry*, vol. 85, no. 3, pp. 1290–1294, 2013.

[8] J. Wang, X. Yu, S. V. Boriskina, and B. M. Reinhard, "Quantification of differential ErbB1 and ErbB2 cell surface expression and spatial nanoclustering through plasmon coupling," *Nano Letters*, vol. 12, no. 6, pp. 3231–3237, 2012.

[9] F. Xu *et al.*, "Membrane-wrapped nanoparticles probe divergent roles of GM3 and phosphatidylserine in lipid-mediated viral entry pathways," *PNAS*, vol. 115, no. 39, pp. E9041–E9050, 2018.

[10] W. Shan *et al.*, "Systematic evaluation of the toxicity and biodistribution of virus mimicking mucus-penetrating DLPC-NPs as oral drug delivery system," *International Journal of Pharmaceutics.*, vol. 530, no. 1–2, pp. 89–98, 2017.

[11] M. Somiya, Q. Liu, and S. Kuroda, "Current Progress of Virus-mimicking Nanocarriers for Drug Delivery," *Nanotheranostics*, vol. 1, no. 4, pp. 415–429, 2017.

[12] H. Wang, J. Yu, X. Lu, and X. He, "Nanoparticle systems reduce systemic toxicity in cancer treatment," *Nanomedicine*, vol. 11, no. 2, pp. 103–106, 2016.

[13] E. S. Abamor, A. M. Allahverdiyev, M. Bagirova, and M. Rafailovich, “Meglumine antımoniate-TiO2@Ag nanoparticle combinations reduce toxicity of the drug while enhancing its antileishmanial effect,” *Acta Tropica*, vol. 169, pp. 30–42, 2017.

[14] X. xiao He *et al.*, “Bioconjugated nanoparticles for DNA protection from cleavage,” *Journal of American Chemical Society*, vol. 125, no. 24, pp. 7168–7169, 2003.

[15] Y. Xiao, K. Shi, Y. Qu, B. Chu, and Z. Qian, “Engineering Nanoparticles for Targeted Delivery of Nucleic Acid Therapeutics in Tumor,” *Molecular Therapy - Methods and Clinical Development.*, vol. 12, no. March, pp. 1–18, 2019.

[16] Y. Ding *et al.*, “Gold nanoparticles for nucleic acid delivery,” *Molecular Therapy*, vol. 22, no. 6, pp. 1075–1083, 2014.

[17] P. Foroozandeh and A. A. Aziz, “Insight into Cellular Uptake and Intracellular Trafficking of Nanoparticles,” *Nanoscale Research Letters*, vol. 13, 2018.

[18] P. Guo *et al.*, “Nanoparticle elasticity directs tumor uptake,” *Nature Communication*, vol. 9, no. 1, pp. 1–9, 2018.

[19] X. Xie, J. Liao, X. Shao, Q. Li, and Y. Lin, “The Effect of shape on Cellular Uptake of Gold Nanoparticles in the forms of Stars, Rods, and Triangles,” *Scientific Reports*, vol. 7, no. 1, pp. 1–9, 2017.

[20] P. Paolo *et al.*, “Exploiting Endocytosis for Nanomedicines,” 2014.

[21] S. Zhang, H. Gao, and G. Bao, “Physical Principles of Nanoparticle Cellular Endocytosis,” *ACS Nano*, vol. 9, no. 9, pp. 8655–8671, 2015.

[22] F. Marano, S. Hussain, F. Rodrigues-Lima, A. Baeza-Squiban, and S. Boland, “Nanoparticles: Molecular targets and cell signalling,” *Archives of Toxicology*, vol. 85, no. 7, pp. 733–741, 2011.

[23] D. G. Capco and Y. Chen, *Nanomaterial impacts on Cell Biology and Medicine*, vol. 811. 2014.

[24] N. J. Sniadecki, “Minireview: A tiny touch: Activation of cell signaling pathways with magnetic nanoparticles,” *Endocrinology*, vol. 151, no. 2, pp. 451–457, 2010.

[25] A. Prat *et al.*, “Predicting response and survival in chemotherapy-treated triple-negative breast cancer,” *British Journal of Cancer*, vol. 111, no. 8, pp. 1532–1541, 2014.

[26] R. BAZAK, M. HOURI, S. EL ACHY, W. HUSSEIN, and T. REFAAT, “Passive targeting of nanoparticles to cancer: A comprehensive review of the literature,” *Molecular and Clinical Oncology*, vol. 2, no. 6, pp. 904–908, 2014.

[27] R. Ngoune, A. Peters, D. von Elverfeldt, K. Winkler, and G. Pütz, “Accumulating nanoparticles by EPR: A route of no return,” *Journal of Controled Release*, vol. 238,

pp. 58–70, 2016.

[28] Reprinted from publication title vol. 40, no. 1, pp. 233–245, 2011, L. Y. T. Chou, K. Ming, and W. C. W. Chan, "Strategies for the intracellular delivery of nanoparticles," *Chemica. Society Reviews*, copyright (2011).

[29] M. S. Franco, "'Active Targeting of Breast Cancer Cells Using Nanocarriers,'" *Modern Applications in Pharmacy and Pharmacology.*, vol. 1, no. 2, pp. 1–4, 2018.

[30] B. Huang, W. D. Abraham, Y. Zheng, S. C. Bustamante López, S. S. Luo, and D. J. Irvine, "Active targeting of chemotherapy to disseminated tumors using nanoparticle-carrying T cells," *Science Translational Medicine*, vol. 7, no. 291, 2015.

[31] S. A. Costa, D. Mozhdehi, M. J. Dzuricky, F. J. Isaacs, E. M. Brustad, and A. Chilkoti, "Active Targeting of Cancer Cells by Nanobody Decorated Polypeptide Micelle with Bio-orthogonally Conjugated Drug," *Nano Letters*, vol. 19, no. 1, pp. 247–254, 2019.

[32] N. Muhamad, T. Plengsuriyakarn, and K. Na-Bangchang, "Application of active targeting nanoparticle delivery system for chemotherapeutic drugs and traditional/herbal medicines in cancer therapy: A systematic review," *International Journal of Nanomedicine*, vol. 13, pp. 3921–3935, 2018.

[33] Stockhofe K, Postema JM, Schieferstein H, Ross TL. Radiolabeling of Nanoparticles and Polymers for PET Imaging. Pharmaceuticals (Basel, Switzerland). 2014 ;7(4):392-418. DOI: 10.3390/ph7040392.

[34] T. M. Brand, M. Iida, C. Li, and D. L. Wheeler, "The nuclear epidermal growth factor receptor signaling network and its role in cancer.," *Discovery Medicine*, vol. 12, no. 66, pp. 419–32, 2011.

[35] S. Y. Lin *et al.*, "Nuclear localization of EGF receptor and its potential new role as a transcription factor," *Nature Cell Biology.*, vol. 3, no. 9, pp. 802–808, 2001.

[36] R. . Nicholson, J. M. . Gee, and M. . Harper, "EGFR and cancer prognosis," *European Journal of Cancer*, vol. 37, pp. 9–15, 2002.

[37] S. Akhtar and I. F. Benter, "The role of epidermal growth factor receptor in diabetes-induced cardiac dysfunction," *BioImpacts*, vol. 3, no. 1, pp. 5–9, 2013.

[38] G. Bethune, D. Bethune, N. Ridgway, and Z. Xu, "Jtd-02-01-048," 2010.

[39] T. Mitsudomi and Y. Yatabe, "Epidermal growth factor receptor in relation to tumor development: EGFR gene and cancer," *FEBS Journal*, vol. 277, no. 2, pp. 301–308, 2010.

[40] G. Selvaggi *et al.*, "Epidermal growth factor receptor overexpression correlates with a poor prognosis in completely resected non-small-cell lung cancer," *Annals of*

Oncology, vol. 15, no. 1, pp. 28–32, 2004.

[41] P. S. Grudinkin, V. V. Zenin, A. V. Kropotov, V. N. Dorosh, and N. N. Nikolsky, "EGF-induced apoptosis in A431 cells is dependent on STAT1, but not on STAT3," *European Journal Cell Biology*, vol. 86, no. 10, pp. 591–603, 2007.

[42] N. M. Jackson and B. P. Ceresa, "EGFR-mediated apoptosis via STAT3," *Experimental Cell Research*, vol. 356, no. 1, pp. 93–103, 2017.

[43] J. Ryu *et al.*, "Paradoxical induction of growth arrest and apoptosis by EGF via the up-regulation of PTEN by activating Redox factor-1/Egr-1 in human lung cancer cells," *Oncotarget*, vol. 8, no. 3, pp. 4181–4195, 2016.

[44] K. Kim, H. G. Wu, and S. R. Jeon, "Epidermal growth factor-induced cell death and radiosensitization in epidermal growth factor receptor-overexpressing cancer cell lines," *Anticancer Research*, vol. 35, no. 1, pp. 245–254, 2015.

[45] J. S. Rush, L. M. Quinalty, L. Engelman, D. M. Sherry, and B. P. Ceresa, "Endosomal accumulation of the activated epidermal growth factor receptor (EGFR) induces apoptosis," *Journal of Biological Chemistry*, vol. 287, no. 1, pp. 712–722, 2012.

[46] B. P. Ceresa, "Spatial regulation of epidermal growth factor receptor signaling by endocytosis," *International Journal of Molecular Sciences*, vol. 14, no. 1, pp. 72–87, 2013.

[47] H. J. Kim, L. J. Taylor, and D. Bar-Sagi, "Spatial Regulation of EGFR Signaling by Sprouty2," *Current Biology*, vol. 17, no. 5, pp. 455–461, 2007.

[48] B.-Z. Shilo, "Regulating the dynamics of EGF receptor signaling in space and time," *Development*, vol. 132, no. 18, pp. 4017–4027, 2005.

[49] M. A. Soliman *et al.*, "Temporal regulation of EGF signalling networks by the scaffold protein Shc1," *Nature*, vol. 499, no. 7457, pp. 166–171, 2013.

[50] M. Amessou *et al.*, "Spatio-temporal regulation of EGFR signaling by the Eps15 homology domain-containing protein 3 (EHD3)," *Oncotarget*, vol. 7, no. 48, 2016.

[51] E. Moradi, D. Vllasaliu, M. Garnett, F. Falcone, and S. Stolnik, "Ligand density and clustering effects on endocytosis of folate modified nanoparticles," *RSC Advances*, vol. 2, no. 7, pp. 3025–3033, 2012.

[52] K. Perica, A. Tu, A. Richter, J. G. Bieler, M. Edidin, and J. P. Schneck, "Magnetic field-induced t cell receptor clustering by nanoparticles enhances t cell activation and stimulates antitumor activity," *ACS Nano*, vol. 8, no. 3, pp. 2252–2260, 2014.

[53] L. Wu, X. Yu, A. Feizpour, and B. M. Reinhard, "Nanoconjugation: A materials approach to enhance epidermal growth factor induced apoptosis," *Biomaterials Science*, vol. 2, no. 2, pp. 156–166, 2014.

[54] L. Wu, F. Xu, and B. M. Reinhard, “Nanoconjugation prolongs endosomal signaling of the epidermal growth factor receptor and enhances apoptosis,” *Nanoscale*, vol. 8, no. 28, pp. 13755–13768, 2016.

[55] X. Gao, J. Dong, and X. Zhang, “The effect of nanoparticle size on endocytosis dynamics depends on membrane-nanoparticle interaction,” *Molecular Simulation*, vol. 41, no. 7. Taylor & Francis, pp. 531–537, 2015.

[56] P. Vedantam, G. Huang, and T. R. J. Tzeng, “Size-dependent cellular toxicity and uptake of commercial colloidal gold nanoparticles in DU-145 cells,” *Cancer Nanotechnology*, vol. 4, no. 1–3, pp. 13–20, 2013.

[57] H. Yuan and S. Zhang, “Effects of particle size and ligand density on the kinetics of receptor-mediated endocytosis of nanoparticles,” *Applied Physics Letters*, vol. 96, no. 3, pp. 1–4, 2010.

[58] K. Li and M. Schneider, “Quantitative evaluation and visualization of size effect on cellular uptake of gold nanoparticles by multiphoton imaging-UV/Vis spectroscopic analysis,” *Journal of Biomedical Optics*, vol. 19, no. 10, p. 101505, 2014.

[59] I. Kalashnikova *et al.*, “Nanoparticle delivery of curcumin induces cellular hypoxia and ROS-mediated apoptosis: Via modulation of Bcl-2/Bax in human neuroblastoma,” *Nanoscale*, vol. 9, no. 29, pp. 10375–10387, 2017.

[60] O. S. Adeyemi, D. A. Otohinoyi, O. J. Awakan, and A. A. Adeyanju, “Cellular apoptosis of HFF cells by inorganic nanoparticles not susceptible to modulation by Toxoplasma gondii infection in vitro,” *Toxicology in Vitro*, vol. 54, no. October 2018, pp. 280–285, 2019.

[61] R. F. De Araújo *et al.*, “Apoptosis in human liver carcinoma caused by gold nanoparticles in combination with carvedilol is mediated via modulation of MAPK/Akt/mTOR pathway and EGFR/FAAD proteins,” *International Journal of Oncology*, vol. 52, no. 1, pp. 189–200, 2018.

[62] B. D. Chithrani and W. C. W. Chan, “Elucidating the mechanism of cellular uptake and removal of protein-coated gold nanoparticles of different sizes and shapes,” *Nano Letters*, vol. 7, no. 6, pp. 1542–1550, 2007.

[63] F. Lu, S.-H. Wu, Y. Hung, and C.-Y. Mou, “Size Effect on Cell Uptake in Well-Suspended, Uniform Mesoporous Silica Nanoparticles,” *Small*, vol. 5, no. 12, pp. 1408–1413, 2009.

[64] S. H. Wang, C. W. Lee, A. Chiou, and P. K. Wei, “Size-dependent endocytosis of gold nanoparticles studied by three-dimensional mapping of plasmonic scattering images,” *Journal of Nanobiotechnology*, vol. 8, pp. 1–13, 2010.

[65] J. REJMAN, V. OBERLE, I. S. ZUHORN, and D. HOEKSTRA, “Size-dependent internalization of particles via the pathways of clathrin- and caveolae-mediated

endocytosis," *Biochemistry Journal*, vol. 377, no. 1, pp. 159–169, 2004.

[66] L. Shang, K. Nienhaus, and G. U. Nienhaus, "Engineered nanoparticles interacting with cells: size matters."

[67] A. Tsourkas, D. R. Elias, A. Poloukhtine, and V. Popik, "Effect of ligand density, receptor density, and nanoparticle size on cell targeting.," *Nanomedicine Nanotechnology, Biology and Medicine*, vol. 9, no. 2, pp. 194–201, 2013.

[68] S. Salatin, S. Maleki Dizaj, and A. Yari Khosroushahi, "Effect of the surface modification, size, and shape on cellular uptake of nanoparticles," *Cell Biology International*, vol. 39, no. 8, pp. 881–890, 2015.

[69] Y. J. Lee, E.-Y. Ahn, and Y. Park, "Shape-dependent cytotoxicity and cellular uptake of gold nanoparticles synthesized using green tea extract," *Nanoscale Research Letters*, vol. 14, no. 1, p. 129, 2019.

[70] F. Murad, "Nitric Oxide: The Coming of the Second Messenger," *Rambam Maimonides Medical Journal*, vol. 2, no. 2. 2011.

[71] J. F. Kerwin, J. R. Lancaster, and P. L. Feldman, "Nitric Oxide: A New Paradigm for Second Messengers," *Journal of Medicinal Chemistry*, vol. 38, no. 22, pp. 4343–4362, 1995.

[72] H. Schulman, "Nitric oxide: A spatial second messenger," *Molecular Psychiatry*, vol. 2, no. 4, pp. 296–299, 1997.

[73] A. Martínez-Ruiz and S. Lamas, "Two decades of new concepts in nitric oxide signaling: From the discovery of a gas messenger to the mediation of nonenzymatic posttranslational modifications," *IUBMB Life*, vol. 61, no. 2, pp. 91–98, 2009.

[74] M. S. Weng, J. H. Chang, W. Y. Hung, Y. C. Yang, and M. H. Chien, "The interplay of reactive oxygen species and the epidermal growth factor receptor in tumor progression and drug resistance," *Journal of Experimental and Clinical Cancer Research*, vol. 37, no. 1, pp. 1–11, 2018.

[75] Reprinted from publication title vol. 24, no. 10, pp. 1–25, 2015. A. Manuscript and O. Stress, "ROS Function in Redox Signaling and Oxidative Stress Michael," *Current Biology* copyright (2015).

[76] V. N. Zaporozhan, A. I. Gozhenko, T. V. Korneenko, and V. G. Dubinina, "Role of nitric oxide in tumor growth," *Uspekhi fiziologicheskikh nauk*, vol. 35, no. 1, pp. 66–82, 2004.

[77] H. W. Lo *et al.*, "Nuclear interaction of EGFR and STAT3 in the activation of the iNOS/NO pathway," *Cancer Cell*, vol. 7, no. 6, pp. 575–589, 2005.

[78] A. J. Burke, F. J. Sullivan, F. J. Giles, and S. A. Glynn, "The yin and yang of nitric oxide in cancer progression," *Carcinogenesis*, vol. 34, no. 3, pp. 503–512, 2013.

[79] H. Vahora, M. A. Khan, U. Alalami, and A. Hussain, “The Potential Role of Nitric Oxide in Halting Cancer Progression Through Chemoprevention,” *Journal of Cancer Prevention*, vol. 21, no. 1, pp. 1–12, 2016.

[80] J. Zhang *et al.*, “ROS and ROS-Mediated Cellular Signaling,” *Oxidative Medicine and Cellular Longevity*, vol. 2016, no. Figure 1, pp. 1–18, 2016.

[81] M. Russwurm and D. Koesling, “NO activation of guanylyl cyclase,” *EMBO Journal*, vol. 23, no. 22, pp. 4443–4450, 2004.

[82] S. Ambs and S. A. Glynn, “Candidate pathways linking inducible nitric oxide synthase to a basal-like transcription pattern and tumor progression in human breast cancer,” *Cell Cycle*, vol. 10, no. 4, pp. 619–624, 2011.

[83] X. Feng *et al.*, “S-nitrosylation of ERK inhibits ERK phosphorylation and induces apoptosis,” *Scientific Reports*, vol. 3, 2013.

[84] D. A. Wink, Y. Vodovotz, J. Laval, F. Laval, M. W. Dewhirst, and J. B. Mitchell, “The multifaceted roles of nitric oxide in cancer,” *Carcinogenesis*, vol. 19, no. 5, pp. 711–721, 1998.

[85] I. Afanas’ev, “Reactive oxygen species signaling in cancer: comparison with aging.,” *Aging and Disease*, vol. 2, no. 3, pp. 219–30, 2011.

[86] T. H. Truong and K. S. Carroll, “Redox Regulation of EGFR Signaling Through Cysteine Oxidation,” *Biochemistry*, vol. 51, no. 50, pp. 9954–9965, 2012.

[87] B. Liu and A. H. Neufeld, “Activation of epidermal growth factor receptor signals induction of nitric oxide synthase-2 in human optic nerve head astrocytes in glaucomatous optic neuropathy,” *Neurobiology and Disease*, vol. 13, no. 2, pp. 109–123, 2003.

[88] Y. G. Yuan, Q. L. Peng, and S. Ggurunathan, “Silver nanoparticles enhance the apoptotic potential of gemcitabine in human ovarian cancer cells: Combination therapy for effective cancer treatment,” *International Journal of Nanomedicine*, vol. 12, pp. 6487–6502, 2017.

4.2 Chapter 2

[1] A. Sorkin, Internalization and Degradation of the EGF Receptor, Humana Press, New York, 2008 Search PubMed .

[2] M. A. Lemmon, Z. M. Bu, J. E. Ladbury, M. Zhou, D. Pinchasi, I. Lax, D. M. Engelman and J. Schlessinger, EMBO Journal, 1997, 16, 281–294 CrossRef CAS PubMed .

[3] E. Raymond, S. Faivre and J. P. Armand, Drugs, 2000, 60, 15–23 CrossRef CAS PubMed .

[4] K. Abe and H. Saito, Brain Research, 1992, 587, 102–108 CrossRef CAS PubMed .

[5] A. Barrie, E. Chieregatti, M. Miloso, F. Benfenati and F. Valtorta, Molecular Pharmacology, 1996, 49, 399–403 CAS .

[6] K. J. Rowland, P. M. Choi and B. W. Warner, Seminars in Pediatric Surgery 2013, 22, 101–111 CrossRef PubMed .

[7] L. Wang, H. C. Chiang, W. Wu, B. Liang, Z. Xie, X. Yao, W. Ma, S. Du and Y. Zhong, Proceedings of National Academy of Sciences U. S. A., 2012, 109, 16743–16748 CrossRef CAS PubMed .

[8] D. K. Armstrong, S. H. Kaufmann, Y. L. Ottaviano, Y. Furuya, J. A. Buckley, J. T. Isaacs and N. E. Davidson, Cancer Research, 1994, 54, 5280–5283 CAS .

[9] G. N. Gill and C. S. Lazar, Nature, 1981, 293, 305–307 CrossRef CAS PubMed .

[10] T. J. Kottke, A. L. Blajeski, L. M. Martins, P. W. Mesner Jr., N. E. Davidson, W. C. Earnshaw, D. K. Armstrong and S. H. Kaufmann, Journal of Biological chemistry, 1999, 274, 15927–15936 CrossRef CAS .

[11] A. Tomas, C. E. Futter and E. R. Eden, Trends in Cell Biology, 2014, 24, 26–34 CrossRef CAS PubMed .

[12] B. P. Ceresa, International Journal of Molecular Science, 2013, 14, 72–87 CrossRef CAS PubMed .

[13] J. S. Rush, L. M. Quinalty, L. Engelman, D. M. Sherry and B. P. Ceresa, Journal of Biological Chemistry, 2012, 287, 712–722 CrossRef CAS .

[14] D. C. Hyatt and B. P. Ceresa, Experimental Cell Research, 2008, 314, 3415–3425 CrossRef CAS PubMed .

[15] B. P. Ceresa and S. L. Schmid, Curr. Opin. Cell Biology, 2000, 12, 204–210 CrossRef CAS PubMed .

[16] A. M. Master and A. Sen Gupta, Nanomedicine, 2012, 7, 1895–1906 CrossRef CAS.

[17] C. L. Tseng, T. W. Wang, G. C. Dong, S. Yueh-Hsiu Wu, T. H. Young, M. J. Shieh, P. J. Lou and F. H. Lin, Biomaterials, 2007, 28, 3996–4005 CrossRef CAS PubMed .

[18] M. Gao, H. Su, G. Lin, S. Li, X. Yu, A. Qin, Z. Zhao, Z. Zhang and B. Z. Tang, Nanoscale, 2016, 8, 15027–15032 RSC .

[19] S. Kuroda, J. Tam, J. A. Roth, K. Sokolov and R. Ramesh, International Journal of Nanomedicine, 2014, 9, 3825–3839 CAS .

[20] A. Verma and F. Stellacci, Small, 2010, 6, 12–21 CrossRef CAS PubMed .

[21] C. C. Fleischer and C. K. Payne, Accounts of Chemical Research, 2014, 47, 2651–2659 CrossRef CAS PubMed .

[22] P. Wang, X. Wang, L. Wang, X. Hou, W. Liu and C. Chen, Science and Technology of Advanced Materials, 2015, 16, 034610 CrossRef PubMed .

[23] Y. Hao, X. Yang, S. Song, M. Huang, C. He, M. Cui and J. Chen, Nanotechnology, 2012, 23, 045103 CrossRef PubMed .

[24] C. Grabinski, N. Schaeublin, A. Wijaya, H. D'Couto, S. H. Baxamusa, K. Hamad-Schifferli and S. M. Hussain, ACS Nano, 2011, 5, 2870–2879 CrossRef CAS PubMed .

[25] L. Wu and B. M. Reinhard, Biomaterials Science, 2014, 2, 156–166 RSC .

[26] L. Wu, F. Xu and B. M. Reinhard, Nanoscale, 2016, 8, 13755–13768 RSC .

[27] H. C. Kolb, M. G. Finn and K. B. Sharpless, Angewandte Chemie International Edition, 2001, 40, 2004–2021 CrossRef CAS PubMed .

[28] J. Wang, S. V. Boriskina, H. Wang and B. M. Reinhard, ACS Nano, 2011, 5, 6619 CrossRef CAS PubMed .

[29] J. N. Anker, W. P. Hall, O. Lyandres, N. C. Shah, J. Zhao and R. P. Van Duyne, Nature Materials, 2008, 7, 442–453 CrossRef CAS PubMed .

[30] M. J. Pollitt, G. Buckton, R. Piper and S. Brocchini, RSC Advances, 2015, 5, 24521–24527 RSC.

[31] M. Lundqvist, J. Stigler, G. Elia, I. Lynch, T. Cedervall and K. A. Dawson, Proceedings in National Academy of Science U. S. A., 2008, 105, 14265–14270 CrossRef CAS PubMed .

[32] D. Docter, D. Westmeier, M. Markiewicz, S. Stolte, S. K. Knauer and R. H. Stauber, Chemical Society Reviews, 2015, 44, 6094–6121 RSC .

[33] K. Hamad-Schifferli, Nanomedicine, 2015, 10, 1663–16674 CrossRef CAS PubMed.

[34] M. Krajewska, H.-G. Wang, S. Krajewski, J. M. Zapata, A. Shabaik, R. Gascoyne and J. C. Reed, Cancer Research, 1997, 57, 1605–1613 CAS .

[35] G. M. Cohen, Biochemistry Journal, 1997, 326, 1–16 CrossRef CAS PubMed .

[36] H. R. Stennicke and G. S. Salvesen, Biochimica et Biophysica Acta, 1998, 1387, 17–31 CrossRef CAS .

[37] N. M. Jackson and B. P. Ceresa, Exp. Cell Research, 2017, 356, 93–103 CAS .

[38] E. C. Cho, J. Xie, P. A. Wurm and Y. Xia, Nano Letters, 2009, 9, 1080–1084 CrossRef CAS PubMed .

[39] L. Vigderman and E. R. Zubarev, Chemistry of Materials, 2013, 25, 1450–1457 CrossRef CAS .

[40] C. Huang, Y. Zhang, H. Yuan, H. Gao and S. Zhang, Nano Letters, 2013, 13, 4546–4550 CrossRef CAS PubMed .

[41] R. Agarwal, V. Singh, P. Jurney, S. V. Sreenivasan and K. Roy, Proceedings of National Academy of Science U. S. A., 2013, 110, 17247–17252 CrossRef CAS PubMed.

[42] X. Liu, F. Wu, Y. Tian, M. Wu, Q. Zhou, S. Jiang and Z. Niu, Scientific Reports, 2016, 6, 24567 CrossRef CAS PubMed .

[43] H. Yang, Z. Chen, L. Zhang, W. Y. Yung, K. C. Leung, H. Y. Chan and C. H. Choi, Small, 2016, 12, 5178–5189 CrossRef CAS PubMed .

[44] S. Zhang, J. Li, G. Lykotrafitis, G. Bao and S. Suresh, Advanced Materials, 2009, 21, 419–424 CrossRef CAS PubMed .

[45] J. Rejman, V. Oberle, I. S. Zuhorn and D. Hoekstra, Biochemistry Journal, 2004, 377, 159–169 CrossRef CAS PubMed .

[46] W. Zhang, Y. Ji, X. Wu and H. Xu, ACS Applied Materials and Interfaces, 2013, 5, 9856–9865 CAS .

[47] A. Manke, L. Wang and Y. Rojanasakul, BioMed Research International, 2013, 2013, 942916 Search PubMed .

[48] T. Xia, M. Kovochich, J. Brant, M. Hotze, J. Sempf, T. Oberley, C. Sioutas, J. I. Yeh, M. R. Wiesner and A. E. Nel, Nano Letters, 2006, 6, 1794–1807 CrossRef CAS PubMed .

[49] A. S. Lavado, V. M. Chauhan, A. A. Zen, F. Giuntini, D. R. Jones, R. W. Boyle, A. Beeby, W. C. Chan and J. W. Aylott, Nanoscale, 2015, 7, 14525–14531 RSC .

[50] K. T. Butterworth, J. A. Coulter, S. Jain, J. Forker, S. J. McMahon, G. Schettino, K. M. Prise, F. J. Currell and D. G. Hirst, Nanotechnology, 2010, 21, 295101 CrossRef CAS PubMed .

[51] Y. Pan, A. Leifert, D. Ruau, S. Neuss, J. Bornemann, G. Schmid, W. Brandau, U. Simon and W. Jahnen-Dechent, Small, 2009, 5, 2067–2076 CrossRef CAS PubMed .

[52] P. V. AshaRani, G. Low Kah Mun, M. P. Hande and S. Valiyaveettil, ACS Nano, 2009, 3, 279–290 CrossRef CAS PubMed .

[53] P. Chairuangkitti, S. Lawanprasert, S. Roytrakul, S. Aueviriyavit, D. Phummiratch, K. Kulthong, P. Chanvorachote and R. Maniratanachote, Toxicology In Vitro, 2013, 27, 330–338 CrossRef CAS PubMed .

[54] Y. Shi, F. Wang, J. He, S. Yadav and H. Wang, Toxicology Letters, 2010, 196, 21–27 CrossRef CAS PubMed .

[55] P. Manna, M. Ghosh, J. Ghosh, J. Das and P. C. Sil, Nanotoxicology, 2012, 6, 1–21 CrossRef CAS PubMed .

[56] X. Wang, Genes Dev., 2001, 15, 2922–2933 CAS .

[57] Y. S. Bae, S. W. Kang, M. S. Seo, I. C. Baines, E. Tekle, P. B. Chock and S. G. Rhee, Journal of Biological Chemistry, 1997, 272, 217–221 CrossRef CAS PubMed .

[58] G. J. DeYulia Jr., J. M. Carcamo, O. Borquez-Ojeda, C. C. Shelton and D. W. Golde, Proceedings In National Academy of Science U. S. A., 2005, 102, 5044–5049 CrossRef PubMed .

[59] S. Zhuang and R. G. Schnellmann, American Journal of Physiology Renal Physiology, 2004, 286, F858–F865 CrossRef PubMed .

[60] H. A. Woo, S. H. Yim, D. H. Shin, D. Kang, D. Y. Yu and S. G. Rhee, Cell, 2010, 140, 517–528 CrossRef CAS PubMed .

[61] E. K. Pias and T. Y. Aw, Cell Death and Differentiation, 2002, 9, 1007–1016 CrossRef CAS PubMed .

[62] E. K. Pias and T. Y. Aw, FASEB J., 2002, 16, 781–790 CrossRef CAS PubMed .

[63] M. L. Circu and T. Y. Aw, Biochimica et Biophysica Acta, 2012, 1823, 1767–1777 CrossRef CAS PubMed .

[64] Y. H. Han, S. H. Kim, S. Z. Kim and W. H. Park, J. Cellular Biochemistry, 2008, 104, 862–878 CrossRef CAS PubMed .

[65] S. Y. Sun, Cancer Biology and Therapy, 2010, 9, 109–110 CrossRef PubMed .

[66] M. C. Krishna, D. A. Grahame, A. Samuni, J. B. Mitchell and A. Russo, Proceedings In National Academy of Science U. S. A., 1992, 89, 5537–5541 CrossRef CAS .

[67] W. Kudo, M. Yamato, K. Yamada, Y. Kinoshita, T. Shiba, T. Watanabe and H. Utsumi, Free Radical Research, 2008, 42, 505–512 CrossRef CAS PubMed .

[68] B. P. Ceresa, Endocytic Trafficking of the Epidermal Growth Factor Receptor in Transfomed Cells, in Breast Cancer - Carcinogenesis, Cell Growth and Signalling Pathways, ed. M. Gunduz, 2011 Search PubMed .

[69] M. Jovic, M. Sharma, J. Rahajeng and S. Caplan, Histology and Histopathology, 2010, 25, 99–112 CAS .

[70] R. Hartmann, M. Weidenbach, M. Neubauer, A. Fery and W. J. Parak, Angewandte Chemie International Edition, 2015, 54, 1365–1368 CrossRef CAS PubMed .

[71] E. W. Miller, O. Tulyathan, E. Y. Isacoff and C. J. Chang, Nature Chemistry and Biology, 2007, 3, 263–267 CrossRef CAS PubMed .

[72] J. Couet, M. Sargiacomo and M. P. Lisanti, Journal of Biological Chemistry, 1997, 272, 30429–30438 CrossRef CAS PubMed .

[73] S. Agelaki, M. Spiliotaki, H. Markomanolaki, G. Kallergi, D. Mavroudis, V. Georgoulias and C. Stournaras, Cancer Biology and Therapy, 2009, 8, 1470–1477 CrossRef CAS PubMed .

[74] W. Y. Park, J. S. Park, K. A. Cho, D. I. Kim, Y. G. Ko, J. S. Seo and S. C. Park, Journal of Biological Chemistry, 2000, 275, 20847–20852 CrossRef CAS PubMed .

[75] C. R. Chong and P. A. Janne, Nature Medicine, 2013, 19, 1389–1400 CrossRef CAS PubMed .

4.3 Chapter 3

(1) Gill, G. N.; Lazar, C. S. Increase phosphotyrosine content and inhibition of proliferation in EGF-treated A431 cells. *Nature* **1981**, *293*, 305-307.

(2) Kottke, T. J.; Blajeski, A. L.; Martins, L. M.; Mesner Jr., P. W.; Davidson, N. E.; Earnshaw, W. C.; Armstrong, D. K.; Kaufmann, S. H. Comparison of paclitaxel-, 5-Fluoro-2'-deoxyuridine-, and epdiermal growth factor (EGF)-induced apoptosis. *Journal of Biological Chemistry* **1999**, *274*, 15927-15936.

(3) Armstrong, D. K.; Kaufmann, S. H.; Ottaviano, Y. L.; Furuya, Y.; Buckley, J. A.; Isaacs, J. T.; Davidson, N. E. Epidermal growth factor-mediated apoptosis of MDA-MB-468 human breast cancer cells. *Cancer Research* **1994**, *54*, 5280-5283.

(4) Wu, L.; Reinhard, B. M. Nanoconjugation: a materials approach to enhance epidermal growth factor induced apoptosis. *Biomaterials Science* **2014**, *2*, 156-166.

(5) Wu, L.; Xu, F.; Reinhard, B. M. Nanoconjugation prolongs endosomal signaling of the epidermal growth factor receptor and enhances apoptosis. *Nanoscale* **2016**, *8*, 13755-13768.

(6) Khanehzar, A.; Fraire, J. C.; Xi, M.; Feizpour, A.; Xu, F.; Wu, L.; Coronado, E. A.; Reinhard, B. M. Nanoparticle-Cell Interactions Induced Apoptosis: A Case Study with Nanoconjugated Epidermal Growth Factor. *Nanoscale* **2018**, *10*, 6712-6723.

(7) Ceresa, B. P.; Schmid, S. L. Regulation of signal transduction by endocytosis. *Current Opinion in Cell Biology* **2000**, *12*, 204-210.

(8) Hyatt, D. C.; Ceresa, B. P. Cellular localization of the activated EGFR determines its effect on cell growth in MDA-MB-468 cells. *Experimental Cell Research* **2008**, *314*, 3415-3425.

(9) Rush, J. S.; Quinalty, L. M.; Engelman, L.; Sherry, D. M.; Ceresa, B. P. Endosomal Accumulation of the Activated Epidermal Growth Factor Receptor (EGFR) Induces Apoptosis. *The Journal of Biological Chemistry* **2012**, *287*, 712-722.

(10) Ceresa, B. P. Spatial Regulation of Epidermal Growth Factor Receptor Signaling by Endocytosis. *International Journal of Molecular Science* **2013**, *14*, 72-87.

(11) Felsen, D.; Broadbelt, N. V.; Chen, J.; Poppas, D. P. Pressure And Epidermal Growth Factor (EGF) Activate Inducible Nitric Oxide Synthase (iNOS) in Human Renal Epithelial Cells (HKC-8). The *Journal of Urology* **2008**, *179*, 219-220.

(12) Lo, H. W.; Hsu, S. C.; Ali-Seyed, M.; Gunduz, M.; Xia, W.; Bartholomeusz, G.; Shih, J. Y.; Hung, M. C. Nuclear interaction of EGFR and STAT3 in the activation of the iNOS/NO pathway. *Cancer Cell* **2005**, *7*, 575-589.

(13) Liu, B.; Neufeld, A. H. Activation of epidermal growth factor receptor signals induction of nitric oxide synthase-2 in human optic nerve head astrocytes in glaucomatous optic neuropathy. *Neurobiology of Disease* **2003**, *13*, 109-123.

(14) Tuteja, N.; Chandra, M.; Tuteja, R.; Misra, M. K. Nitric Oxide as a Unique Bioactive Signaling Messenger in Physiology and Pathophysiology *Journal of Biomedicine and Biotechnology* **2004**, *2004*, 227-237.

(15) Russwurm, M.; Koesling, D. NO activation of guanylyl cyclase. *EMBO Journal* **2004**, *23*, 4443-4450.

(16) Burke, A. J.; Sullivan, F. J.; Giles, F. J.; Glynn, S. A. The yin and yang of nitric oxide in cancer progression *Carcinogenesis* **2013**, *34*, 503-512.

(17) Ambs, S.; Glynn, S. A. Candidate pathways linking inducible nitric oxide synthase to a basal-like transcription pattern and tumor progression in human breast cancer. *Cell Cycle* **2011**, *10*, 619-624.

(18) Switzer, C. H.; Glynn, S. A.; Cheng, R. Y.; Rifnour, L. A.; Green, J. E.; Ambs, S.; Wink, D. A. S-nitrosylation of EGFR and Src activates an oncogenic signaling network in human basal-like breast cancer. *Molecular Cancer Research* **2012**, *10*, 1203-1215.

(19) Wink, D. A.; Vodovotz, Y.; Laval, J.; Laval, F.; Dewhirst, M. W.; Mitchell, J. B. The multifaceted roles of nitric oxides in cancer. *Carcinogenesis* **1998**, *19*, 711-721.

(20) Cheng, H.; Wang, L.; Mollica, M.; Re, A. T.; Wu, S.; Zuo, L. Nitric Oxide in Cancer Metastasis. *Cancer Letters* **2014**, *353*, 1-7.

(21) Aqil, M.; Elseth, K. M.; Vesper, B. J.; Deliu, Z.; Aydogan, B.; Xue, J.; Radesovich, J. A. Part I-mechanism of adaption: high nitric oxide adapted A549 cells show enhanced DNA damage response and activation of antiapoptotic pathways. *Tumour Biology* **2014**, *35*, 2403-2415.

(22) Leon, J. W.; Jeannin, J. F.; Bettaieb, A. Post-translational modifications induced by nitric oxide (NO): implication in cancer cell apoptosis. *Nitric Oxide* **2008**, 77-83.

(23) Huerta-Yepez, S.; Baritaki, S.; Baay-Guzman, G.; Hernandez-Luna, M. A.; Hernandez-Cueto, A.; Vega, M. I.; Bonavida, B. Contribution of either YY1 or BclXL-induced inhibition by the NO-donor DETANONOate in the reversal of drug resistance, both in vitro and in vivo. YY1 and BclXL are overexpressed in prostate cancer. *Nitrix Oxide* **2013**, *29*, 17-24.

(24) Pervin, S.; Chaudhuri, G.; Singh, R. NO to Breast: When, Why and Why Not? *Current Pharmaceutical Design* **2010**, *16*, 451-462.

(25) Garrido, P.; Shalaby, A.; Walsh, E. M.; Keane, N.; Webber, M.; Keane, M. M.; Sullivan, F. J.; Kerin, M. J.; Callagy, G.; Ryan, A. E.; Glynn, S. A. Impact of inducible nitric oxide synthase (iNOS) expression on triple negative breast cancer outcome and activation of EGFR and ERK signaling pathways. *Oncotarget* **2017**, *8*, 80568-80588.

(26) Firger, J. Nitric Oxide Inhibitors Hit Target for Triple Negative Breast Cancer. *Journal of the National Cancer Institute* **2015**, *107*, djv235.

(27) Jin, Z.; Wang, W.; Jiang, N.; Zhang, L.; Li, Y.; Xu, X.; Cai, S.; Wei, L.; Liu, X.; Chen, G.; Zhou, Y.; Liu, C.; Li, Z.; Jin, F.; Chen, B. Clinical Implications of iNOS Levels in Triple-Negative Breast Cancer Responding to Neadjuvant Chemotherapy. *PLoS One* **2015**, *10*, e130286.

(28) Hickok, J. R.; Thomas, D. D. Nitric Oxide and Cancer Therapy: The Emperor has NO Clothes. *Current Pharmeutical Design* **2010**, *16*, 381-391.

(29) Lala, P. K.; Orucevic, A. Role of nitric oxide in tumor progression: lesson from experimental tumors. *Cancer Metastasis Reviews* **1998**, *17*, 91-106.

(30) Saklimian, R. B.; Achreja, A.; Nagrath, D. Nitric Oxide: The Forgotten Child of Tumor Metabolism. *Trends Cancer* **2017**, *3*, 659-672.

(31) Switzer, C. H.; Ridnour, L. A.; Cheng, R.; Heinecke, J.; Burke, A.; Glynn, S. A.; Ambs, S.; Wink, D. A. S-Nitrosation Mediates Multiple Pathways That Lead to Tumor Progression in Estrogen Receptor-Negative Breast Cancer. *Forum in Immunopathological Disease and Therapy* **2012**, *3*, 117-124.

(32) Badve, S.; Dabbs, D. J.; Schnitt, S. J.; Baehner, F. L.; Decker, T.; Eusebi, V.; Fox, S. B.; Ichihara, S.; Jacquemier, J.; Lakhani, S. R.; Palacios, J.; Rakha, E. A.; Richardson, A. L.; Schmitt, F. C.; Tan, P. H.; Tse, G. M.; Weigelt, B.; Ellis, I. O.; Reis-Filho, J. S. Basal-like and triple-negative breast cancers: a critical review with an emphasis on the implications for pathologists and oncologists. *Modern Pathology* **2011**, *24*, 157-167.

(33) Leidy, J.; Khan, A.; Kandil, D. Basal-like breast cancer: update on clinicopathologic, immunohistochemical, and molecular features. *Archives of Pathology and Laboratory Medicine* **2014**, *138*, 37-43.

(34) Alluri, P.; Newman, L. A. Basal-like and triple-negative breast cancers: searching for positives among many negatives. *Surgical Oncology Clinics of North America* **2014**, *23*, 567-577.

(35) Toft, D. J.; Cryns, V. L. Minireview: Basal-Like Breast Cancer: From Molecular Profiles to Targeted Therapies. *Molecular Endocrinology* **2011**, *25*, 199-211.

(36) Cohen, G. M. Caspase: the executioners of apoptosis. *Biochemical Journal* **1997**, *326*, 1-16.

(37) Mandal, B.; Bhattacherjee, H.; Mittal, N.; Sah, H.; Balabathula, P.; Thoma, L. A.; Wood, G. C. Core-shell-type lipid-polymer hybrid nanoparticles as a drug delivery platform. *Nanomedicine* **2013**, *9*, 474-491.

(38) Gan, H. K.; Walker, F.; Burgess, A. W.; Rigopoulos, A.; Scott, A. M.; Johns, T. G. The Epidermal Growth Factor Receptor (EGFR) Tyrosine Kinase Inhibitor AG1478 Increases the Formation of Inactive Untethered EGFR Dimers. *The Journal of Biological Chemistry* **2007**, *282*, 2840-2850.

(39) Lonne, G. K.; Masoumi, K. C.; Lennartsson, J.; Larsson, C. Protein Kinase Cδ Supports Survival of MDA-MB-231 Breast Cancer Cells by Suppressing the ERK1/2 Pathway. *Journal of Biological Chemistry* **2009**, *284*, 33456-33465.

(40) Janssen, Y. M.; Soultanakis, r.; Steece, K.; Heerdt, E.; Singh, R. J.; Joseph, J.; Kalyanaraman, B. Depletion of nitric oxide causes cell cycle alterations, apoptosis, and oxidative stress in pulmonary cells. *American Journal of Physiology* **1998**, *275*, L1100-L1109.

(41) Kolb, H. C.; Finn, M. G.; Sharpless, K. B. Click Chemistry: Diverse Chemical Function from a Few Good Reactions. *Angewandte Chemie International Edition* **2001**, *40*, 2004-2021.

(42) Hartmann, R.; Weidenbach, M.; Neubauer, M.; Fery, A.; Parak, W. J. Stiffness-dependent in vitro uptake and lysosomal acidification of colloidal particles. *Angewandte Chemie International Edition* **2015**, *54*, 1365-1368.

(43) Yi, X.; Shi, X.; Gao, H. Cellular uptake of elastic nanoparticles. *Physical Review Letters* **2011**, *107*, 098101.

(44) Yi, X.; Gao, H. Cell membrane wrapping of a spherical thin elastic shell. *Soft Matter* **2015**, *11*, 1107.

(45) Yi, X.; Gao, H. Kinetics of receptor-mediated endocytosis of elastic nanoparticles. *Nanoscale* **2017**, *9*, 454-463.

(46) Tang, H.; Ye, H.; Zhang, H.; Zheng, Y. Wrapping of nanoparticles by the cell membrane: the role of interactions between the nanoparticles. *Soft Matter* **2015**, *11*, 8674-8683.

(47) Banguy, X.; Suarez, F.; Argaw, A.; Rabanel, J.-M.; Grutter, P.; Bouchard, J.-F.; Hildgen, P.; Giasson, S. Effect of mechanical properties of hydrogel nanoparticles on macrophage cell uptake. *Soft Matter* **2009**, *5*, 3984-3991.

(48) Fu, P. P.; Xia, Q.; Hwang, H. M.; Ray, P. C.; Yu, H. Mechanism of nanotoxicity: generation of reactive oxygen species. *Journal of Food and Drug Analysis* **2014**, *22*, 67-75.

(49) Manke, A.; Wang, L.; Rojanasakul, Y. Mechanisms of nanoparticle-induced oxidative stress and toxicity. *BioMed research international* **2013**, *2013*, 942916.

(50) Lehman, S. E.; Morris, A. S.; Mueller, P. S.; Salem, A. K.; Grassian, V. H.; Larsen, S. C. Silica nanoparticle-generated ROS as a predictor of cellular toxicity: mechanistic insights and safety by design. *Environmental Science: Nano* **2016**, *3*, 56-66.

(51) Cao, B. J.; Reith, M. E. Nitric oxide scavenger carboxy-PTIO potentiates the inhibition of dopamine uptake by nitric oxide donors. *European Journal of Pharmacology* **2002**, *448*, 27-30.

(52) Vahora, H.; Khan, M. A.; Alalami, U.; Hussain, A. The Potential Role of Nitric Oxide in Halting Cancer Progression Through Chemoprevention. *Journal of Cancer Prevention* **2016**, *21*, 1-12.

(53) Napoli, C.; Paolisso, G.; Casamassimi, A.; Al-Omran, M.; Barbieri, M.; Sommese, L.; Infante, T.; Ignarro, L. J. Effects of nitric oxide on cell proliferation: novel insights. *Journal of the American College of Cardiology* **2013**, *62*, 89-95.

(54) Thomas, D. D.; Ridnour, L. A.; Isenberg, J. S.; Flores-Santana, W.; Switzer, C. H.; Donzelli, S.; Hussain, P.; Vecoli, C.; Paolocci, N.; Ambs, S.; Colton, C. A.; Harris, C. C.; Roberts, D. D.; Wink, D. A. The chemical biology of nitric oxide: implications in cellular signaling. *Free Radical Biology and Medicine* **2008**, *45*, 18-31.

(55) Castellano, I.; Ercolesi, E.; Palumbo, A. Nitric Oxide Affects ERK Signaling through Down-Regulation of MAP Kinase Phosphatase Levels during Larval Development of the Ascidian Ciona intestinalis. *PLoS ONE* **2014**, *9*, e102907.

(56) Yang, S.; Guo, L.; Su, Y.; Wen, J.; Du, J.; Li, X.; Liu, Y.; Feng, J.; Xie, Y.; Bai, Y.; Wang, H.; Liu, Y. Nitric oxide balances osteoblast and adipocyte lineage differentiation via the JNK/MAPK signaling pathway in periodontal ligament stem cells. *Stem Cell Research and Therapy* **2018**, *9*, 118.

(57) Doronzo, G.; Viretto, M.; Russo, I.; Mattiello, L.; Di Martino, L.; Cavalot, F.; Anfossi, G.; Trovati, M. Nitric oxide activates PI3-K and MAPK signalling pathways in human and rat vascular smooth muscle cells: influence of insulin resistance and oxidative stress. *Journal of Atherosclerosis* **2011**, *216*, 44-53.

(58) Browning, D. G.; McShane, M. P.; Marty, C.; Ye, R. D. Nitric Oxide Activation of p38 Mitogen-activated Protein Kinase in 293T Fibroblasts Requires cGMP-dependent Protein Kinase. *Journal of Biological Chemistry* **2000**, *275*, 2811-2816.

(59) Raines, K. W.; Bonini, M. G.; Campbell, S. L. Nitric oxide cell signaling: S-nitrosation of Ras superfamily GTPases. *Cardiovascular Research* **2007**, *75*, 229-239.

(60) Dhanasekaran, D. N.; Reddy, E. P. JNK Signaling in Apoptosis. *Oncogene* **2008**, *27*, 6245-6251.

(61) Liu, J.; Lin, A. Role of JNK activation in apoptosis: a double-edged sword. *Cell Research* **2005**, *15*, 36-42.

(62) Park, H. S.; Mo, J. S.; Choi, E. J. Nitric oxide inhibits an interaction between JNK1 and c-Jun through nitrosylation. *Biochemical and Biophysical Research Communications* **2006**, *351*, 281-286.

(63) Shen, H. M.; Liu, Z. G. JNK signaling pathway is a key modulator in cell death mediated by reactive oxygen and nitrogen species. *Free Radical Biology and Medicine* **2006**, *40*, 928-939.

5 Curriculum Vitae